Realising SQUID on Tip - Atomic Force Microscopy (SoT - AFM)
Uitenbroek, Dennis

Citation
Uitenbroek, D. (2022). *Realising SQUID on Tip - Atomic Force Microscopy (SoT - AFM)*.

Version: Not Applicable (or Unknown)
License: License to inclusion and publication of a Bachelor or Master thesis in the Leiden University Student Repository
Downloaded from: https://hdl.handle.net/1887/3453244

Note: To cite this publication please use the final published version (if applicable).

Realising SQUID on Tip - Atomic Force Microscopy (SoT - AFM)

Thesis

submitted in partial fulfillment of the requirements for the degree of

Master of Science
in
Physics

Author :	Dennis Uitenbroek BSc
Student ID :	s1697552
Supervisor :	Prof. dr. Jan Aarts
	Dr. Kaveh Lahabi
2nd corrector :	Dr. Milan Allan

Leiden, The Netherlands, August 21, 2022

Realising SQUID on Tip - Atomic Force Microscopy (SoT - AFM)

Dennis Uitenbroek BSc

Huygens-Kamerlingh Onnes Laboratory, Leiden University
P.O. Box 9500, 2300 RA Leiden, The Netherlands

August 21, 2022

Abstract

SQUID on tip microscopy provides a way of investigating all sorts of physics. SQUIDs are sensitive to both magnetic fields and temperature. By placing a SQUID on a tip the opportunity is enabled to accurately and locally measure magnetic fields and temperature with nanometre spatial resolution. Current SQUID on tip microscopes do not have proper height control, this leads to limited sensitivity and limited spatial resolution.
This thesis presents a solution to this problem by placing a SQUID on an Atomic Force Microscopy (AFM) tip. This combination provides effective height control for the SQUID on tip, and due to the AFM properties topographic information is gained.
In this thesis, a method is designed to realise this combination. The method is based on starting with a commercially available cantilever (Akiyama-Probe) and sputter deposition several layers on top. First, an insulating layer is sputtered that separates the two electrical circuits, and on top of that four conductive layers are sputtered to create the desired SQUID.
Two techniques are implemented to create a SQUID on the tip, either mill the SQUID using Focussed Ion Beam (FIB) milling or directly write the SQUID using Electron Beam Induced Deposition (EBID).
This thesis mainly focuses on creating electrical connections to the AFM cantilever tip. Besides this main topic, preliminary tests were performed for fabricating EBID SQUIDs on an AFM tip.

Contents

1 Introduction **1**
1.1 SQUID 1
1.2 Scanning SQUID and SQUID on Tip 2
1.3 Applications 3
1.3.1 Scanning SQUID by Hilgenkamp's Group 3
1.3.2 Scannning SQUID by Moler's Group 4
1.3.3 SQUID on Tip by Zeldov's Group 5
1.3.4 SQUID on Tip by Poggio's Group 6
1.4 Magnetic Sensitivity and Resolution 7
1.5 Thermal Sensitivity and Resolution 7
1.6 Overcoming the Limitations of Current SoT Imaging 9

2 Working Principle of SQUID-based Imaging **11**
2.1 Magnetic Sensitivity 11
2.2 Thermal Sensitivity 12
2.3 Parameters for SQUID sensitivity 13
2.3.1 Magnetic Transfer Function 13
2.3.2 Magnetic Modulation Depth 14
2.3.3 Thermal Transfer Function 14
2.3.4 Thermal Modulation Depth 14

3 Designs and methods **15**
3.1 Basic Idea 15
3.2 Choosing AFM Probes 16
3.2.1 Akiyama-Probe Specifications 17
3.3 Electrical Contacts 19
3.3.1 Sputtering 19
3.3.2 Etching 22
3.3.3 Deposition During Etching 23
3.3.4 Etcher Sample Holder 24

3.3.5 Shorted Electrical Contacts 31
3.4 SQUID on Tip 34
3.4.1 FIB SQUIDs 34
3.4.2 EBID SQUIDs 35
3.4.3 Preliminary Tests on an AFM Tip 37

4 Conclusion & Outlook 39

A EBID Planar Devices Parameters 43

Chapter 1

Introduction

In today's condensed matter physics electrical currents, magnetic fields, and temperature are three major physical properties of interest. A SQUID on tip measures these three properties in a sensitive and non-invasive manner. The current problem with this technique is a lack of height control. A solution to this problem is combining SQUID on tip with Atomic Force Microscopy (AFM) or Scanning Tunnelling Microscopy (STM). In addition, this combination also provides topographical information.

Combining these is not trivial, a combination of lithography and Focussed Ion Beam (FIB) milling for example cannot be used. In our research group, two methods of fabrication are presently being implemented to create a SQUID on a commercially available tip. They are Focussed Ion Beam (FIB) milling and Electron Beam Induced Deposition (EBID). The current challenge is to create electrical connections for the read-out of the SQUID reaching towards the apex of the AFM tip.

This thesis mainly focuses on making electrical contacts, and in parallel, we try to optimize the design for EBID SQUIDs.

This chapter provides the introduction to this project. The principle of a SQUID is briefly explained. After this, the difference between a scanning SQUID and a SQUID on tip is explained. Next, we discuss four applications of both scanning SQUIDs and SQUIDs on tips. The relation between the scan height and the magnetic and thermal sensitivity and resolution is explained. The problem with current SQUID on tips is the lack of proper height control, this limits both the magnetic and thermal sensitivity and resolution. At the end of this chapter, a solution is described to overcome the limitations of the current SQUID on tips.

1.1 SQUID

A SQUID (Superconducting Quantum Interference Device) is a superconducting loop with two non-superconducting parts in it. These non-superconducting parts are called weak links. These can for example consist of an insulator or a normal metal. In figure 1.1

a schematic image of a SQUID is shown. In yellow is the superconducting loop and in red are the two weak links. The principle of a SQUID is explained in the theory chapter.

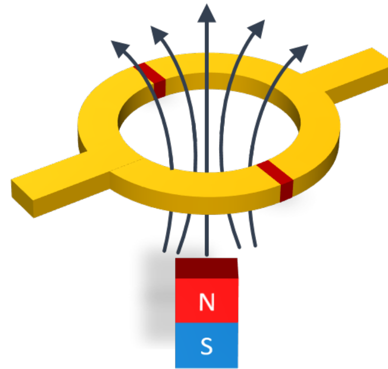

Figure 1.1: *Schematic image of a SQUID. The superconducting loop is shown in yellow and the two weak links are shown in red. A magnet is illustrated with its magnetic flux lines.*

SQUIDs are sensitive to magnetic fields, this physical principle is explained in section 2.1. Besides their magnetic sensitivity, SQUIDs are also thermally sensitive. This principle is explained in section 2.2.

Currently, SQUIDs are seen as one of the most sensitive existing measurement devices. Probing magnetic and thermal phenomena on the nano-scale is crucial to our understanding of condensed matter physics. By moving a SQUID above a surface a magnetic and thermal image of the device can be made. Using this, electrical currents can also be studied.

1.2 Scanning SQUID and SQUID on Tip

Two techniques to move a SQUID above the surface of a device are scanning SQUID microscopy and SQUID on tip microscopy. Both are interesting techniques because they are non-invasive and they are sensitive to both magnetic fields and temperature. The non-invasiveness is essential to be able to image quantum states. If the techniques would be invasive they would destroy the quantum state.

In the case of a scanning SQUID, a pickup loop is scanned over the surface and a SQUID is used to measure the magnetic flux indirectly. This is shown in figure 1.2a-b.

The other technique, SQUID on Tip, is a more direct way of imaging the surface. This technique eliminates the need for the pickup loop by scanning the SQUID directly above the surface. This method can achieve orders of magnitude higher spatial resolution than other techniques currently available. Examples of both scanning SQUIDs and SQUID on tip measurements have been published. An example of a SQUID on tip is shown in figure 1.2c-d.

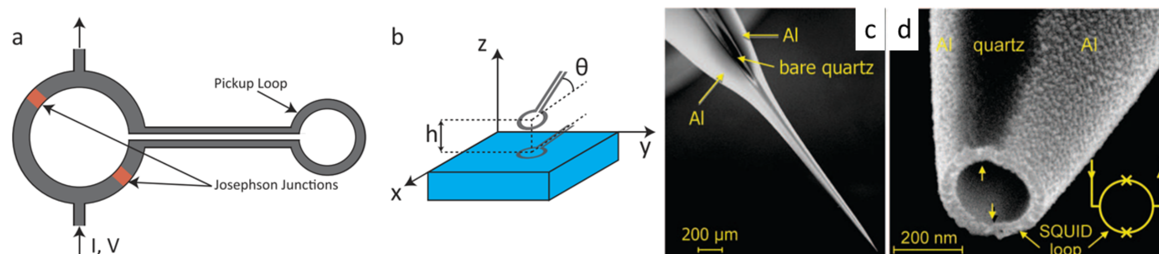

__Figure 1.2:__ The principle of a scanning SQUID is shown in (a) and (b). In figure (a), the pickup loop is shown which is directly in the same circuit as the SQUID. In (b), the pickup loop above the surface of a device is shown. The pickup loop can be moved in all directions. In (c) the apex of a quartz tip is shown. (d) Is an SEM image of the end of the tip, where the SQUID is. The two yellow arrows mark the weak links of the SQUID. Figures (a) and (b) adapted from [1] and figures (c) and (d) from [2].

1.3 Applications

Two applications of scanning SQUIDs and two applications of SQUID on tips are listed below. The papers provide examples of the current achieved resolution and sensitivity of these techniques. The limitations of the techniques in each of the papers are briefly mentioned.

1.3.1 Scanning SQUID by Hilgenkamp's Group

An example of the usage of a scanning SQUID is by Hilgenkamp et al. [3]. In this paper, a SQUID with a 3 µm × 5 µm pickup loop is scanned at a height of approximately 5 µm above a YBCO sample surface at an angle of 30°. Lots of vortices can be seen in figure 1.3. The image in figure 1.3a is taken at a temperature of 4 K with a magnetic field present of 6.93 µT. After this image, the sample is warmed up again above T_c and cooled again in the same way. The sample edge is visible at the left of the images.

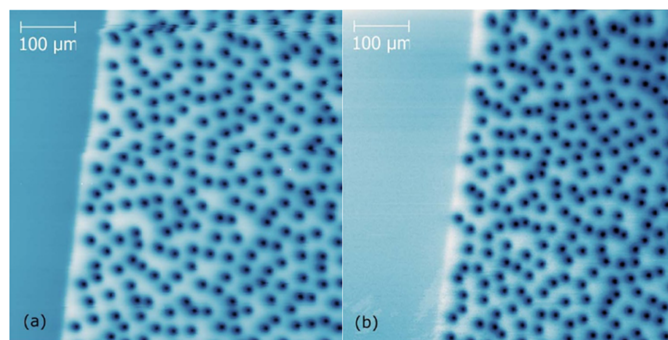

__Figure 1.3:__ A sample of YBCO magnetically imaged with a scanning SQUID. Lots of vortices are visible. At first, the sample is cooled to 4 K with a magnetic field of 6.93 µT present (a). After this magnetic image, the sample is warmed up again above T_c and cooled in the same way (b). [3]

These magnetic images are only possible to make using a scanning SQUID close to the surface. The SQUID size and the distance to the surface (scan height) determine the possible resolution.

1.3.2 Scannning SQUID by Moler's Group

The second application of a scanning SQUID is shown in a paper by Moler et al. [4]. In this paper, a sample with a $LaAlO_3/SrTiO_3$ (LAO/STO) interface is studied for the coexistence of ferromagnetism and superconductivity. A scanning SQUID is used with micrometre-scale spatial resolution to measure the magnetic fields (magnetometry) and the susceptibility of the sample to a small locally applied a.c. magnetic field (susceptometry).

Figure 1.4a shows a magnetometry image and figure 1.4b a susceptometry image of an LAO/STO interface. The ferromagnetic behaviour is seen as many static spatially separated dipoles that show no temperature dependence over the measured temperature range (20 - 100 mK). The susceptometry signal is generated by superconducting electrons that screen the local applied field and is related to the local density of electrons in the superconducting condensate. [4]

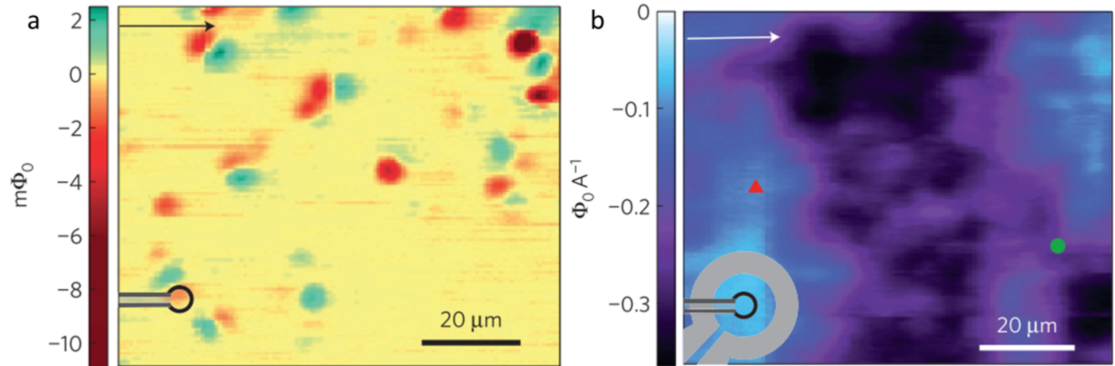

Figure 1.4: *The LAO/STO interface is imaged using a scanning SQUID. Both the magnetic fields (a) are measured and the susceptibility of the sample to a small locally applied a.s. magnetic field (b). The magnetic image shows spatially separated dipoles without temperature dependence. The susceptometry signal is generated by superconducting electrons that screen the local applied field. In both images, the size of the pickup loop is indicated. [4]*

In this paper, the sensitivity of the SQUID limits the visible dipole moments. The paper estimates the electron density associated with the ferromagnetic, diamagnetic, and paramagnetic signals. These density calculations are also limited by spatial resolution. To further study the interplay of these normally incomparable states measurements with higher spatial resolution are required.

1.3.3 SQUID on Tip by Zeldov's Group

An example of a SQUID on tip is given by Zeldov et al. [5]. Here a SQUID is used on the apex of a sharp quartz pipette with an effective diameter of 104 nm. This tip can be used to make a thermal image. In figure 1.5 two of these images are shown. Figure 1.5 a and b are thermal maps of the wires imaged by an SEM in figures c and d respectively.

Both images have their temperature scale. The wire in figure 1.5a carries a current of 12 nA imaged at a scanning height of about 65 nm. In figure 1.5b the wire carries a current of 3 nA and uses a scan height of about 150 nm. The wire in figure b shows an electrical short at the intersection point.

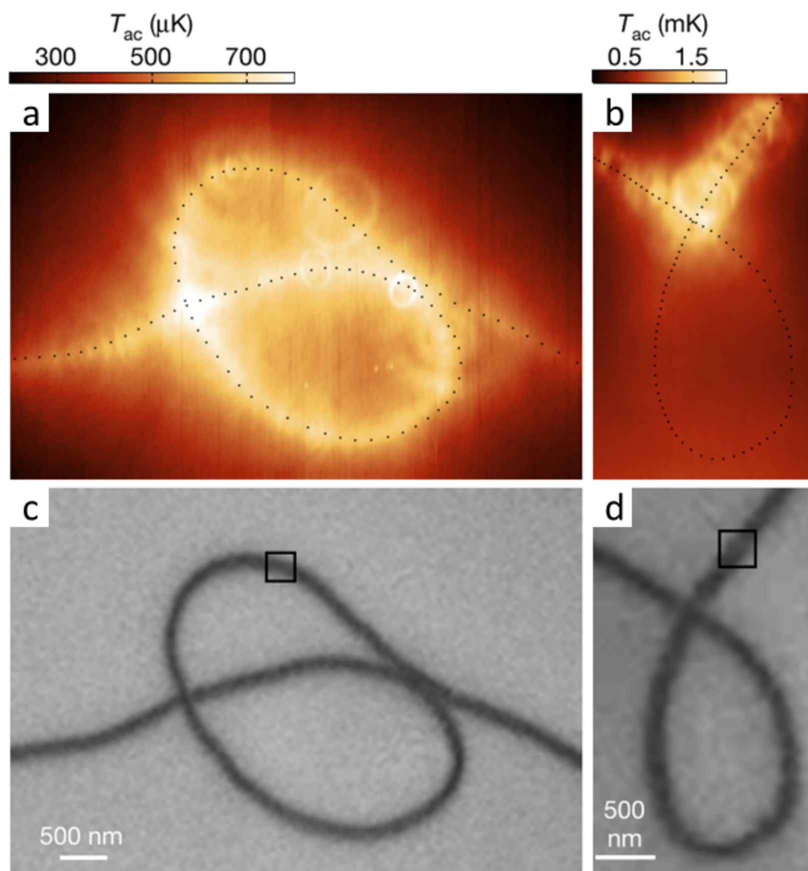

Figure 1.5: *Two wires are thermally imaged and imaged by an SEM. Both wires are imaged with a SQUID with an effective diameter of* 104 nm*. The wire in (a) is thermally imaged while carrying a current of* 12 nA*. The wire in (b) carries a current of* 3 nA*. The intersection of the two wires creates an electrical short. In (c) and (d) two SEM images of the wires are given respectively. [5]*

These dissipations in the order of micro Kelvin are visible when imaged by a SQUID on tip. This would not be possible with any other kind of thermal image.

1.3.4 SQUID on Tip by Poggio's Group

In a very recent paper by Poggio et al. [6] magnetic flux is imaged produced by a superconducting device designed for quantum computing. The flow of superconducting current through the circuit and the locations of trapped magnetic flux are imaged. This shows how the different elements are coupled, which gives an insight into how to optimize the qubit.

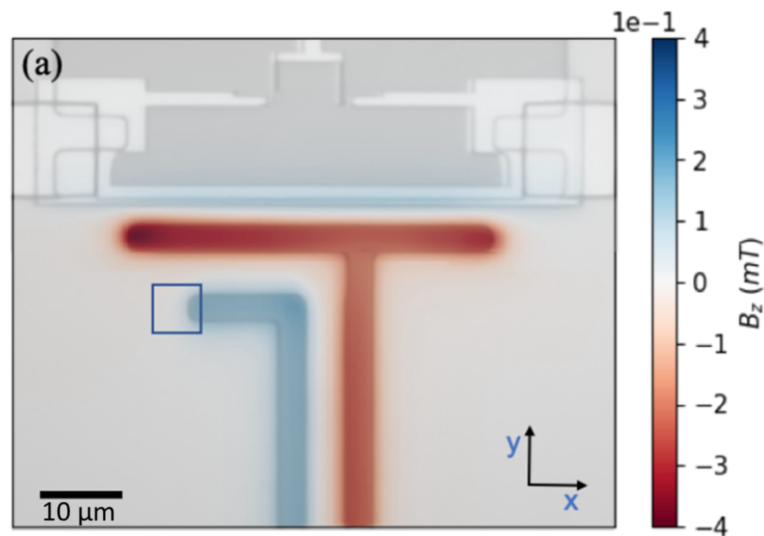

Figure 1.6: *Magnetic field image of a part of a device designed for quantum computing. The magnetic field is locally measured using a SQUID on tip. The magnetic field is given in the colour map. Note the size of the scalebar:* 10 µm. *Adapted from [6].*

In figure 1.6 the magnetic image of the device is shown. The colour map shows the magnetic field measured by a SQUID on tip. This SoT has a diameter of 190 nm and a scan height of 600 nm above the sample. This relativity large scan height compared to the diameter limits the magnetic sensitivity and resolution.

1.4 Magnetic Sensitivity and Resolution

The SQUID is sensitive to magnetic flux, or if the area of the SQUID is known this can be converted into a magnetic field. Two interesting properties of scanning SQUIDs are sensitivity and resolution.

The predicted magnetic sensitivity and resolution are shown in figure 1.7. The left figure shows the ratio of flux through a loop with a diameter (d) and a height above the imaged surface (scan height). The behaviour is plotted for both a current line, a monopole, and a dipole. The sensitivity is best if scan height/ diameter approaches zero. The right figure shows the spatial resolution for again a loop with a diameter (d) and scan height (s). The spatial resolution is best if the fraction scan height/diameter is below 1/2.

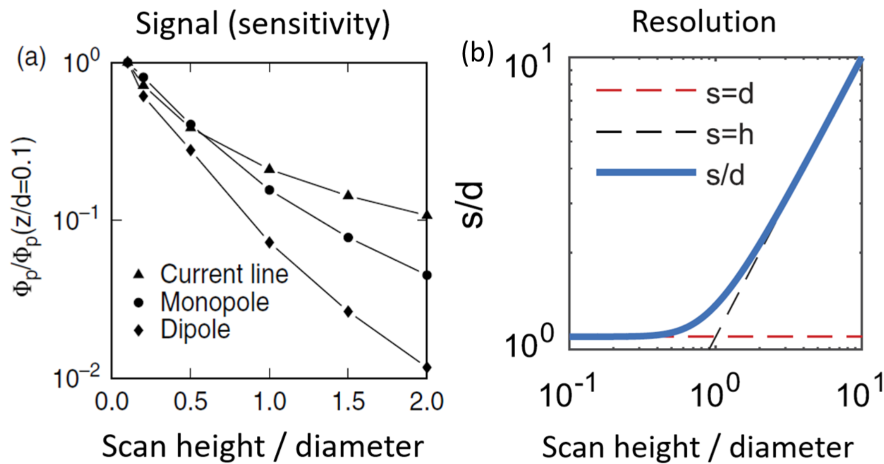

Figure 1.7: *(a) The ratio of flux through a surface with a diameter and scan height [7]. This is plotted for three types of magnetic sources, a current line, a monopole, and a dipole. The sensitivity is best if scan height/ diameter approaches zero. (b) Spatial resolution as a fraction of the diameter as a function of the fraction of scan height (s) and diameter (d). If the fraction of s/d is below 1/2, the best resolution is achieved [1].*

For both the sensitivity and resolution the distance to the surface is an important parameter. If there is no proper height control this limits both the sensitivity and the resolution. This is exactly the case in current scanning SQUID methods, there is no proper height control. This results in limited sensitivity and spatial resolution.

1.5 Thermal Sensitivity and Resolution

The sensitivity and spatial resolution of existing thermal imaging techniques are compared to the thermal sensitivity and resolution of a SQUID on a tip by Zeldov [5]. This is shown in figure 1.8. Here, the different techniques are shown in blue dots. The axis on the left shows the sensitivity of the different techniques as a function of their spatial resolution on the bottom axis. For comparison, an ideal qubit operating at a typical

read-out frequency of 1 GHz operating at 4.2 K is shown as a green diamond with a dashed line. The axis at the top corresponds to the size of the qubit. The axis on the right shows the temperature increase due to 40 fW dissipation. Adapted from Zeldov [5].

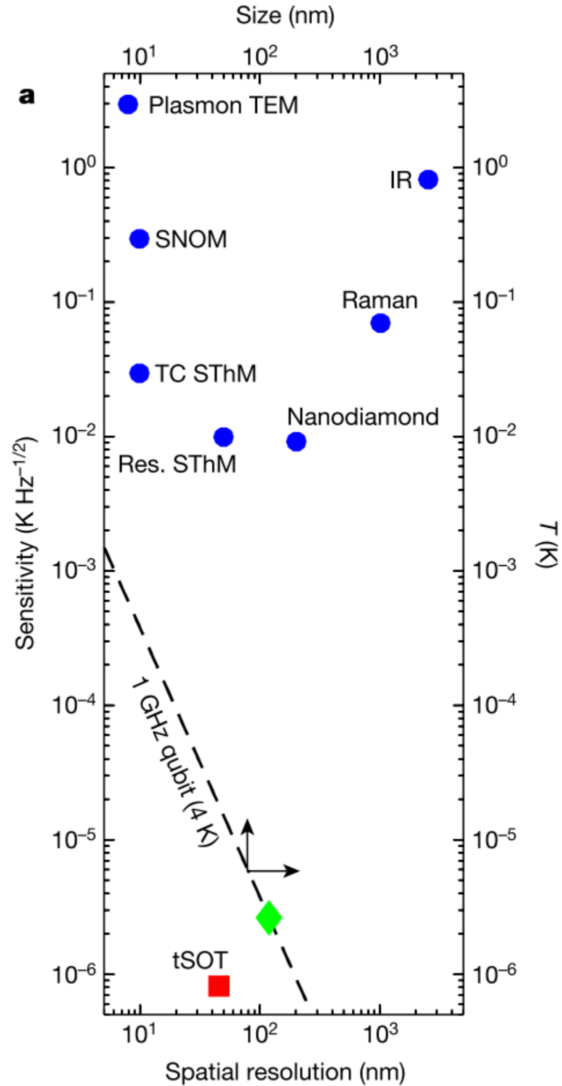

Figure 1.8: *Different thermal imaging techniques compared by Zeldov [5]. The sensitivity of the techniques is shown on the axis on the left. The spatial resolution of the techniques is given on the bottom axis. To compare these values to a qubit the green diamond with a dashed line is included. This is the expected temperature increase (right axis) of a qubit of size (top axis) due to* 40 fW *dissipation operating at* 4.2 K *at a read-out frequency of* 1 GHz*.*

In figure 1.8 it becomes clear that only thermal SQUID on tip measurements are sensitive enough to measure the dissipation of the described qubit. This spatial resolution is orders of magnitudes higher than the other mentioned techniques.

1.6 Overcoming the Limitations of Current SoT Imaging

This project provides a solution to the mentioned limitations. By introducing the combination of a SQUID of an AFM tip there is proper height control. This enables direct height control and therefore the magnetic and thermal sensitivity and spatial resolution can be optimized.

In addition, topographic information is provided which directly follows from the AFM properties. This topographic information automatically provides effective height control. This combination works on a variety of materials, also including insulators. The AFM properties are compatible with various surface morphologies and provide a relatively large scan area, compared to STM for example.

Figure 1.9 shows the described schematic idea. A SQUID is realized on the apex of an AFM tip. This project is about realizing the combination of a SQUID on an AFM tip.

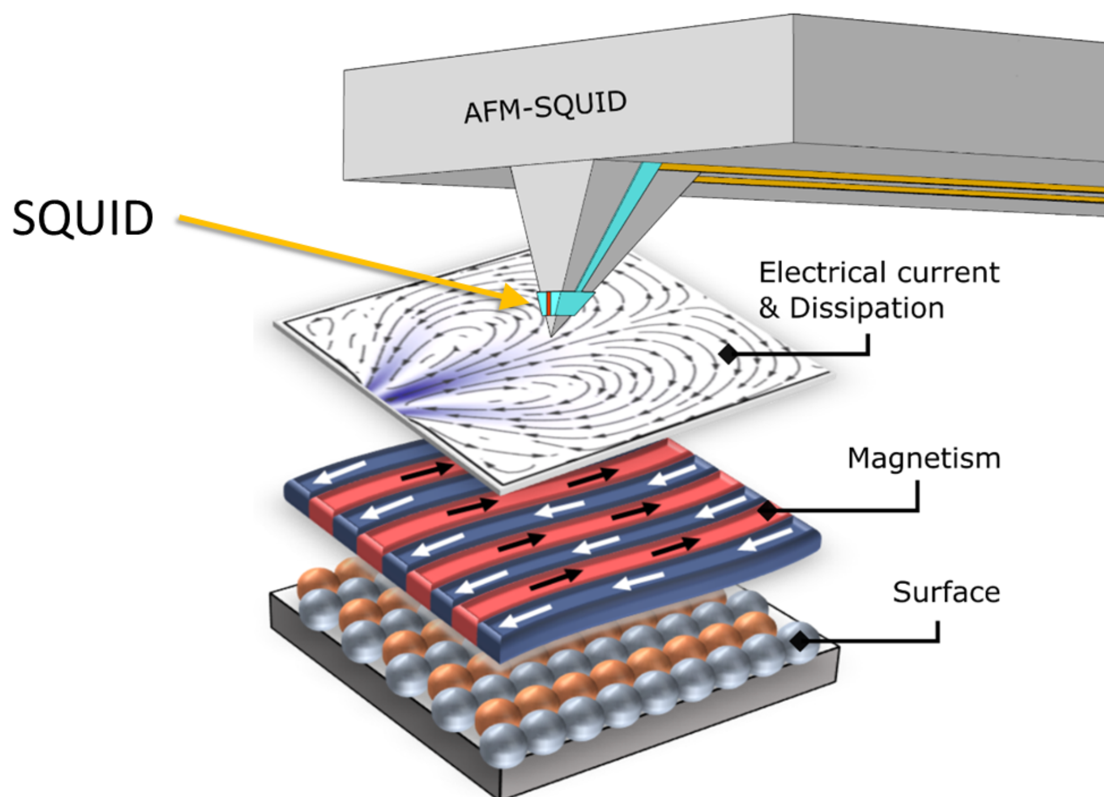

Figure 1.9: *The schematic idea of the project is shown. The challenge is to create a SQUID on the apex of an AFM cantilever. This enables measurements of the surface morphology, magnetism, electrical current, and dissipation.*

Chapter 2

Working Principle of SQUID-based Imaging

This chapter provides a background on SQUID-based imaging techniques. Magnetic and thermal sensitivity and two of their properties, transfer function and modulation depth, are discussed. A background in superconductivity, Josephson Junctions, and SQUIDs is assumed. For explanations about these and much more topics see Clarke and Braginski [8].

2.1 Magnetic Sensitivity

SQUIDs are sensitive to magnetic fields. This is due to the flux quantization in the superconducting loop of the SQUID. If an external magnetic field is applied perpendicular to the loop a screening current begins to circulate. Below half a flux quantum of external flux this screening current cancels out the external flux. The flux enclosed by the loop must be an integer number of flux quanta. Therefore if the external flux is above half a flux quantum the screening current does not cancel the flux anymore instead, it increases the flux to the first flux quantum. This is energetically more favourable than cancelling the external flux.

If in one of the branches of the superconducting loop the current exceeds the critical current, the superconductor will enter a resistive state and across the junction, a voltage is developed. Because the loop has a self-inductance and a shunt resistance across the junction the change in flux is converted to a change in voltage. This results in a non-linear current-voltage relation.

This is graphically shown in figure 2.1. The typical behaviour of a SQUID is shown for a current-voltage characteristic. The critical current (I_c) is the current where the SQUID enters the resistive state. The critical current can change due to external factors, such as an external magnetic field or a change in the temperature of the SQUID. If the critical current is changed this causes a change in the voltage which is developed across

the SQUID. This change in voltage can be measured and calibrated to use a SQUID as a magnetic sensor.

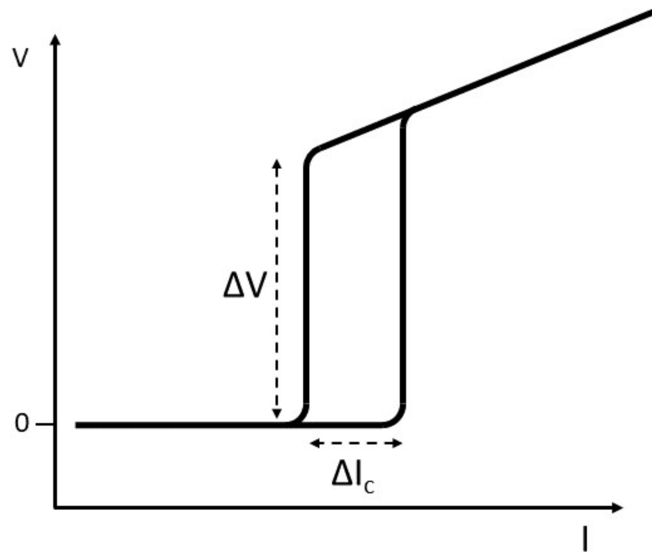

Figure 2.1: *Typical IV curve for a SQUID. The IV curve is nonlinear, the sharp transition is the critical current (I_c). A change in the critical current is caused by an external magnetic field or by a change in temperature. The change in critical current causes a change in the developed voltage across the SQUID.*

2.2 Thermal Sensitivity

The critical current of a superconductor is temperature-dependent. This principle can be used to do thermal measurements with a SQUID. Superconductors have besides a critical current also a critical temperature. Below this critical temperature, the critical current is temperature-dependent. Above this critical temperature, the superconductor is not superconducting and thus the SQUID cannot operate. Typically the critical current of a superconductor is higher for lower temperatures.

In figure 2.1 the change in critical current is shown. This results in a different voltage which is developed for different critical currents i.e. temperatures. By calibrating this behaviour the SQUID can be used as a thermometer below the critical temperature.

2.3 Parameters for SQUID sensitivity

For a SQUID on tip two properties are important. The first is the transfer function and the second is the modulation depth. Both apply to magnetic sensitivity and thermal sensitivity.

2.3.1 Magnetic Transfer Function

The magnetic transfer function of a SQUID is a property that describes the flux-to-voltage response. Or in other words, it is a value for if the superconducting loop encloses one flux quantum how much voltage is developed across the SQUID. This is illustrated in figure 2.2. The SQUID operates around a working point (W), this is the equilibrium value around which the voltage oscillates. A change of external flux in the loop ($\delta\Phi_a$) results in a change in the voltage (δV). The magnetic transfer function (V_Φ) is a fraction of these two: $V_\Phi = \delta V/\delta\Phi_a$. A larger magnetic transfer function enables measurements with higher magnetic resolution.

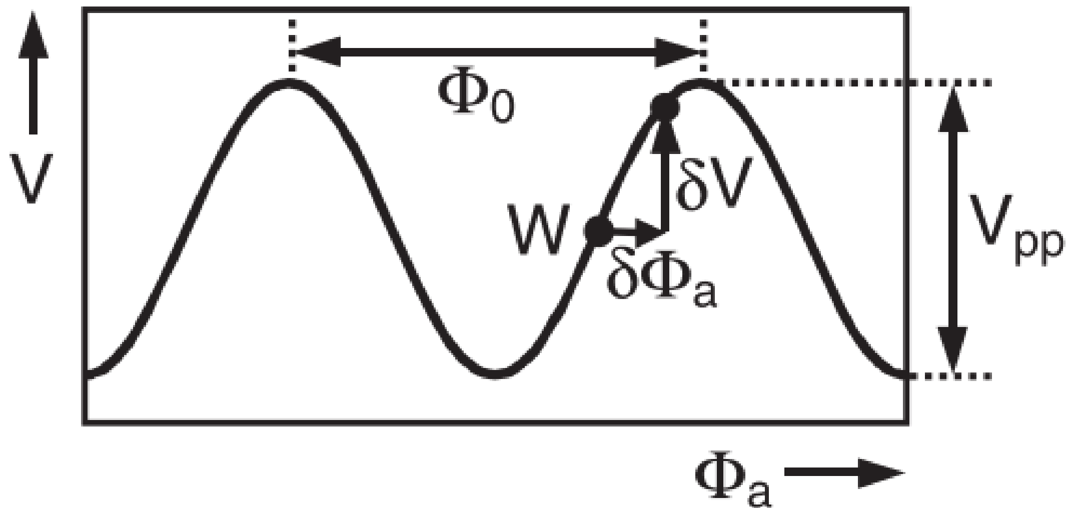

Figure 2.2: *An illustration of the voltage (V) behaviour for increasing external flux (Φ_a) of a SQUID. There is a periodicity of Φ_0 and a peak-to-peak amplitude of V_{pp}. The SQUID operates around a working point (W), a change in flux ($\delta\Phi_a$) creates a change in voltage (δV). [8]*

2.3.2 Magnetic Modulation Depth

The other property is the magnetic modulation depth. This defines the maximum change in external flux that can be measured with the SQUID. This defines up to what region of external flux the SQUID is sensitive.

This is illustrated in figure 2.2. The voltage response of the SQUID has periodic behaviour with periodicity Φ_0. The corresponding peak-to-peak voltage is V_{pp}. The modulation depth is the amount of flux up to which the SQUID is sensitive or translated to voltage, the amount of voltage between a minimum and a maximum of the oscillation, i.e. V_{pp}.

A large modulation depth results in a wider range of flux variation the SQUID can measure.

2.3.3 Thermal Transfer Function

The thermal transfer function is based on the same principle as the magnetic transfer function. The thermal transfer function (V_T) is a fraction between the change in voltage (δV) and the change in temperature (δT): $V_T = \delta V / \delta T$. A larger thermal transfer function enables measurements with higher thermal resolution.

2.3.4 Thermal Modulation Depth

Analogue to the magnetic modulation depth, the thermal modulation depth defines the maximum change in temperature which can be measured using the SQUID. This is the difference in voltage between the minimum and the maximum of the oscillation. As in the case of the magnetic modulation depth, the larger the thermal modulation depth, the wider the range of temperature variation the SQUID can measure.

Chapter 3

Designs and methods

This chapter starts by describing the main idea of how to fabricate a SQUID on an AFM probe. The next step is to choose a specific probe and using this probe, design a method to create electrical contacts all the way to the tip. To create this a sputter mask and an etcher sample holder are designed. In the end, two techniques to fabricate a SQUID on the tip are discussed.

3.1 Basic Idea

The basic idea is to create a SQUID on the tip of an AFM probe. This immediately raises the question of how to make such a micro or nano SQUID on the fragile structure of a sharp AFM probe.

The first option would be to use lithography to make the desired pattern and to sputter the superconducting and metallic layers needed. After this, by using FIB weak links can be formed in between the superconducting parts. However, lithography is not going to work on the tip of an AFM probe. This technique uses chemicals to dissolve the polymer layers both for development and for the lift-off. In the case of an AFM tuning fork probe, the tip is always attached to the tuning fork with some paint or epoxy. The paint or epoxy will also be dissolved when placed in such chemicals and then the tip will be removed from the tuning fork and the tip will be useless.

These problems caused by the lithography process can be circumvented by using FIB milling and/or EBID. A SQUID on an STM tip has been made before using FIB, and a SQUID on a tip using EBID has not been made before. EBID SQUIDs on a planar substrate have been made before.

Now there are two techniques available to create the SQUID on the AFM probe. These are discussed more in detail near the end of this chapter, in section 3.4. The first step is to choose the specific AFM probes which will be used.

3.2 Choosing AFM Probes

As described before it will be an AFM cantilever used in a cryogenic environment. Optical readout is not desirable since this can cause heating and there is a need for a laser. A tuning fork cantilever suitable for cryogenic environments does not have these disadvantages.

When choosing the probes it is a good idea to already think about how to make the electrical connections to the SQUID later on. The probe has to have a geometry workable for this.

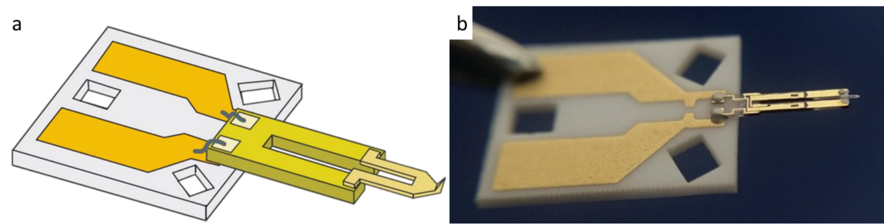

Figure 3.1: *The Akiyama-Probe schematic image on the left and an optical image on the right. (a) A schematic image of the Akiyama-Probes. The tuning fork is mounted on the ceramic base plate and the silicon tip is attached at the end of the tuning fork. (b) A picture of the Akiyama-Probe. The base plate and the tuning fork are clearly visible, the silicon part is also visible as a tiny piece at the end of the tuning fork. Images from [9].*

A cantilever called Akiyama-Probe turns out to have the right geometry to work with. It is schematically shown in figure 3.1a and an optical image is shown in figure 3.1b. It has the right structure to work with, both sides of the tuning fork can be used as separate electrical connections to the tip. The silicon tip is suitable for both FIB and EBID to create the SQUID. However, there are also disadvantages to this cantilever. For example, the silicon tip is a soft material that causes damping. This damping would be lower in the case of a hard tip.

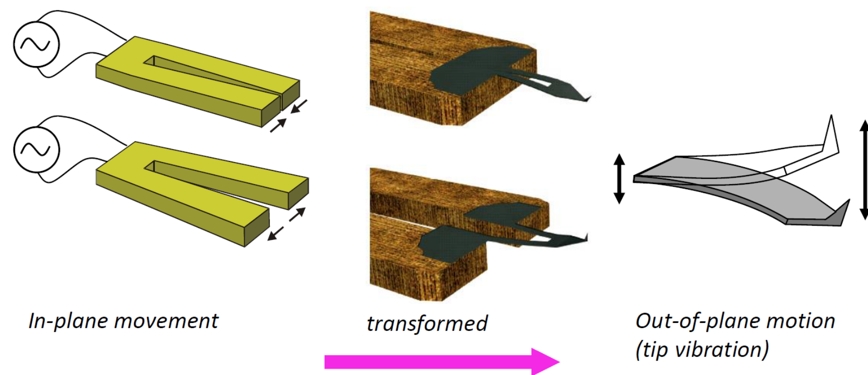

Figure 3.2: *The principle of the Akiyama-Probes is based on an in-plane movement of the quartz tuning fork, created by an oscillating voltage. By the silicon tip, this is transformed into an out-of-plane motion. This results in an oscillating tip. Image from [9].*

The working principle of the Akiyama-Probes is based on applying a voltage to a quartz tuning fork, this creates an in-plane movement. This in-plane movement is transformed into an out-of-plane motion by the shape of the silicon tip. This principle and conversion are shown in figure 3.2.

3.2.1 Akiyama-Probe Specifications

The specifications are taken from the website of Akiyama-Probes [9]. Below is table 3.1, in this table the specifications of the cantilever, tip, and tuning fork are given.

Cantilever	length: 310 µm, thickness: 3.7 µm, width: 30 µm each, n-type, highly doped silicon (0.01 ∼ 0.025 Ωcm)
Tip	AdvancedTEC™-like, tip radius: <15 nm, tip height: 28 µm
Force constant	5 N/m (Si cantilever part)
Tuning fork prongs	thickness (tTF) of 124 µm, width (wTF) of 214 µm
Resonance frequency	33 – 60 kHz

Table 3.1: *In this table the specifications of the cantilever, tip, and tuning fork are given of the used Akiyama-Probes.*

The dimensions of the base plate and the silicon tip are given in figure 3.3. The boxes with cantilevers all come with their own measurement datasheet. For each cantilever, the measured resonance frequency, quality factor, capacitance, and frequency shift are given on this datasheet. The frequency shift is an estimated maximum shift at 20 °C and RH40%.

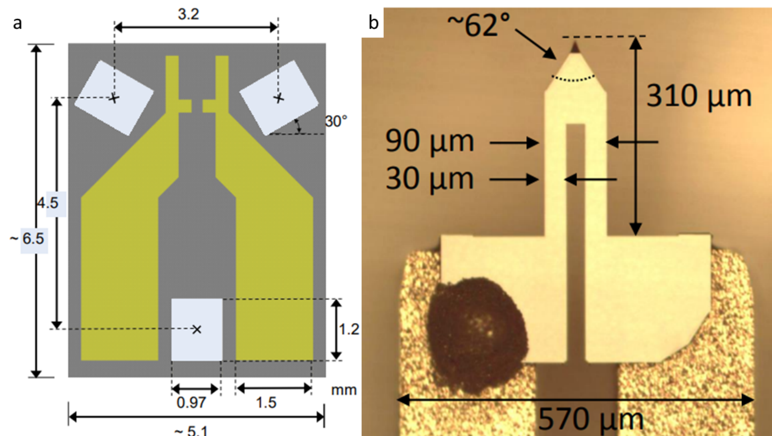

Figure 3.3: *The Akiyama-Probe dimensions of the base plate schematic on the left and the dimensions of the silicon tip on the right. (a) A schematic image of the base plate of the Akiyama-Probes. All dimensions are given in millimetres and angles in degrees. The ceramic plate is shown in grey and the gold contacts are shown in green. (b) An optical image of the silicon tip. Dimensions are given in the image.*

As a reference for the use of an Akiyama cantilever, two images of a paper by Akiyama et al. [10] are cited in figure 3.4. An AFM image of highly oriented pyrolitic graphite (HOPG) and a cross-section across the dotted line is shown in figure 3.4a. The topography of a microelectronic chip is shown in figure 3.4b.

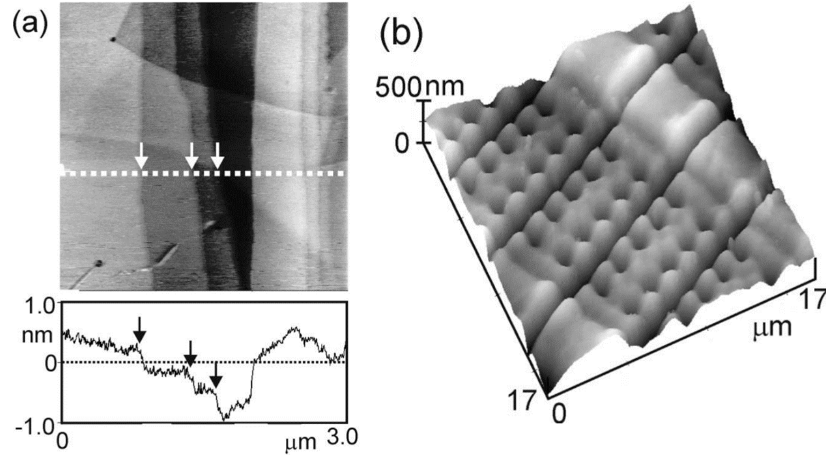

Figure 3.4: *AFM (a) and topographic (b) images made using an Akiyama-Probe as an example. Images and information from Akiyama et al. [10]. (a) AFM image of highly oriented pyrolitic graphite (HOPG) and a cross-sectional view along the dotted line. Monoatomic terraces (arrows) are clearly revealed. (b) Topography of a microelectronic chip imaged in the intermittent contact mode with a probe having a very soft cantilever* (0.01 N/m)*.*

Besides the images in this paper, an AFM topographic image was also made in collaboration with the set-up of a colleague at Leiden University from the Van Ruitenbeek group. Norman Blümel and Jimi de Haan made the topographic image of evaporated gold on mica, the image in figure 3.5.

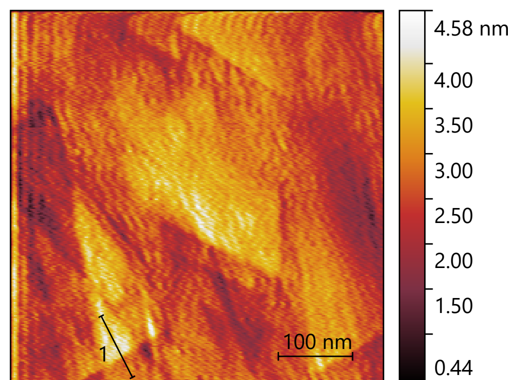

Figure 3.5: *Topographic image of evaporated gold on mica. Image produced by Norman Blümel and Jimi de Haan using an Akiyama-Probe.*

The probes are functional and two techniques to create the necessary SQUIDs are known. There is a challenge in making electrical connections to the end of the tip.

3.3 Electrical Contacts

To use the SQUID at the tip of a probe electrical connections are required from a location where you can wire-bond the connections all the way to the very end of the tip. Again, lithography does not work on these fragile tips. Either the process of lithography itself or the chemicals used during the lift-off will destroy the tip.

3.3.1 Sputtering

Another option to create the electrical contacts is to sputter a conductive layer on the probe. In the method of Matthijs Rog [11], the cantilever is covered by sputtering metals and after that, the conductive layer is cut in two to create two contacts using FIB. This in principle works also on the Akiyama-Probes. However, this method applied to the Akiyama-Probes is extremely challenging. The distance to mill by FIB is way larger and this takes already hours in the case of the STM tips of Matthijs Rog.

The Akiyama-Probes have an electrical circuit to enable tuning fork AFM. A conductive layer sputtered on top would of course short the whole tuning fork circuit. To separate the two electrical circuits an insulating layer can be placed in between. This can be done by firstly sputtering the insulating layer and after this layer sputtering the conductive layers.

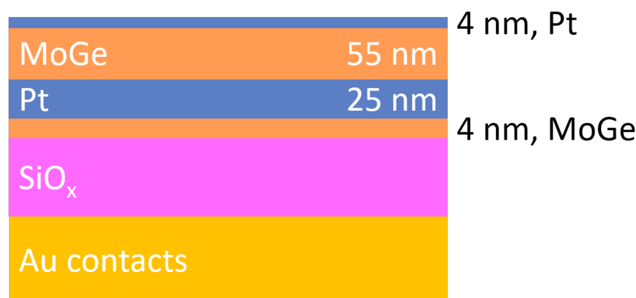

Figure 3.6: *The schematic idea of the stacked layers on the cantilever. At the bottom are the gold AFM contacts, on top of that is an insulating layer of silicon oxide to separate the two electrical circuits. On top are the four conductive layers,* 4 nm *Molybdenum-Germanium (MoGe),* 25 nm *Platinum (Pt),* 55 nm *Molybdenum-Germanium (MoGe), and* 4 nm *Platinum (Pt). The reasoning behind the layers can be found in the text.*

The conductive layers on top of the sputtered insulating layer are held the same as on the STM tips of Matthijs Rog. All layers can be found in figure 3.6, the gold AFM contacts can be seen at the bottom of the image. The insulating layer is a layer of silicon oxide, the thickness of this layer can be chosen as desired. The conductive layers exist out of first a layer of 4 nm Molybdenum-Germanium (MoGe), second a layer of 25 nm Platinum (Pt), third a layer of 55 nm Molybdenum-Germanium (MoGe) and fourth a layer of 4 nm of Platinum (Pt). The first layer of MoGe is used as a sticking layer, without this layer the Platinum would not attach properly to the silicon oxide layer.

The two thicker layers, 25 nm of Platinum and 55 nm of MoGe, will eventually form the SQUID. The MoGe layer will act as the superconductor of the SQUID and at the desired location, the MoGe layer is milled away to create the weak links. At the location of the weak links now the platinum layer is left over which will transport the supercurrent to the other side of the trench. This Platinum now creates a weak link of a normal metal. The last layer, 4 nm of Platinum, is a capping layer. These four conductive layers are sometimes referred to as the multilayer. Further details can be found in the thesis of Matthijs Rog [11].

To eliminate milling on the base plate as well as the first part of the tuning fork a sputter mask is designed. This creates two separate contacts up to the first part of the tuning fork when sputtering the cantilever.

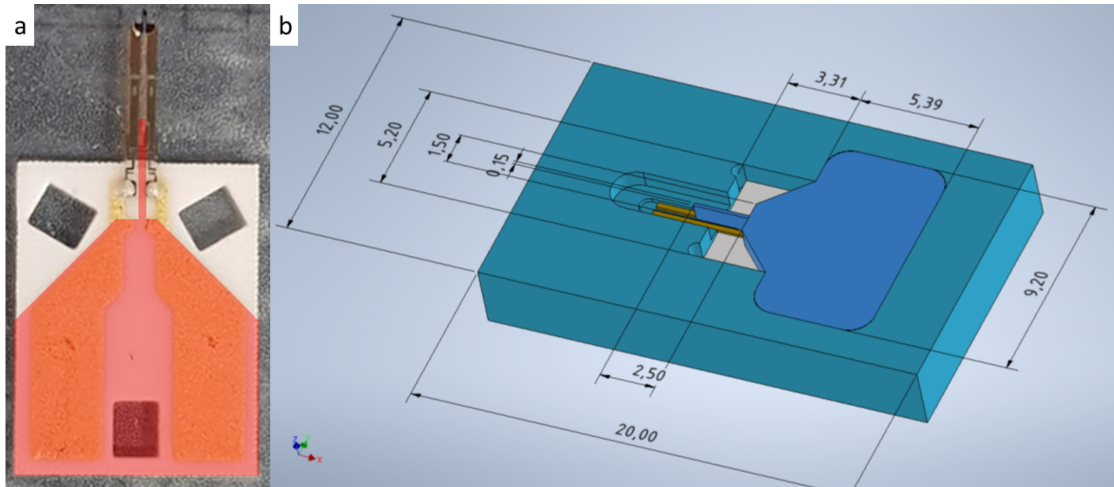

Figure 3.7: *The schematic idea of the sputter mask (a) and the graphical 3D drawing made by the FMD (b).*

The schematic idea of the sputter mask is drawn in figure 3.7a. In red the part that is covered with the sputter mask. As stated before this creates two separate electrical contacts up to the first part of the tuning fork. The part covered with the sputter mask will have no deposition while sputtering. This leaves the main part of the two gold contacts available for the AFM tuning fork measurement. The same idea is drawn in figure 3.7b in graphical 3D software, all measures are given in millimetres in this drawing.

Sputtering is a non-directional process. Therefore any part which is not supported from below will have deposition on the backside. Therefore the sputter mask is also designed to have a part supporting the tuning fork. Otherwise, it would be shorted from the backside.

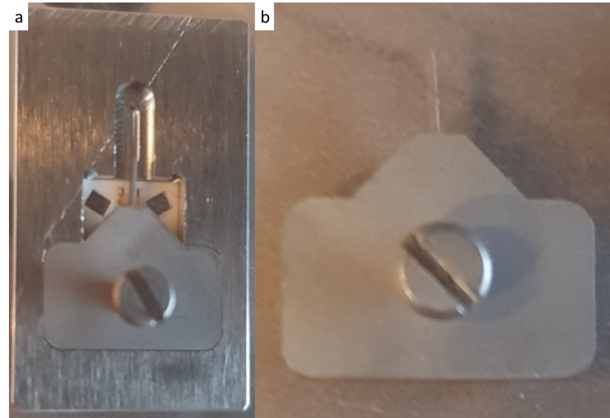

Figure 3.8: *The sputter mask as it is used during sputtering on the left. The stainless steel lid of the sputter mask is on the right. The screw in the lid is only used as a handle. (a) Image of the sputter mask as used during sputtering. The Akiyama-Probe can be seen in between the aluminium holder and the stainless steel lid. (b) An image of the stainless steel lid of the sputter mask.*

Figure 3.8 shows two images, figure 3.8a the mask used during sputtering, and figure 3.8b the stainless steel lid of the sputter mask. The sputter mask covers the part as described in the schematic design with the stainless steel lid. The aluminium holder supports both the base plate and the tuning fork. The screw on the lid is only meant as a handle.

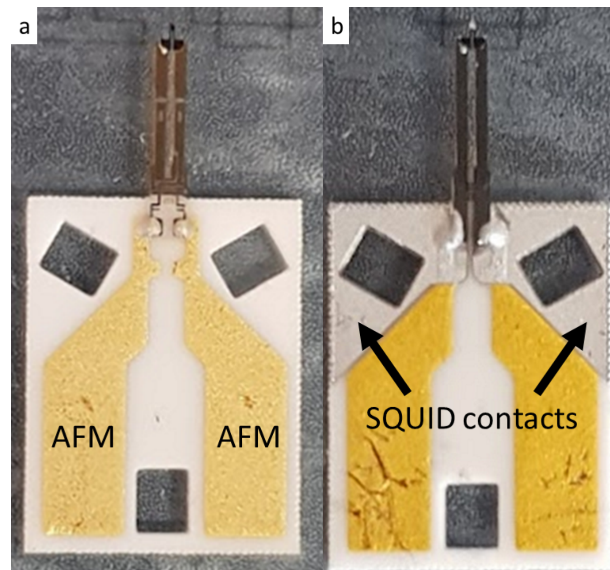

Figure 3.9: *Both an unsputtered (a) and a sputtered (b) cantilever are shown. Both have two gold contacts available for AFM measurements. The sputtered cantilever also has two contacts for SQUID measurements.*

Figure 3.9 shows both a cantilever before sputtering (fig. 3.9a) and after sputtering (fig. 3.9b). Both before and after sputtering the two gold contacts are visible to use for tuning fork AFM measurements. After sputtering the two new SQUID contacts are visible created by the sputter mask.

Only the tip of the Akiyama-Probe is shorting the electrical contacts after sputtering. The tip is too small and too fragile to also cover with a mask. Both the front side and the backside are shorting the circuit. The SQUID is going to be located on the front side. The electrical connections therefore also need to be on this side. This side will be cut into two electrodes using FIB. The backside could also be cut into two pieces using FIB, but this is very time-consuming. To eliminate FIB milling at the backside the conductive layers have to be removed from there. This can be done by etching away the conductive material at the backside.

3.3.2 Etching

The conductive material on the backside is removed by etching the backside with ions. The used etcher uses argon ions to etch. At first, the same method as Matthijs Rog is used. The probe needs to point to the surface of the etcher sample holder to etch the backside. Therefore the probe is placed on a piece of aluminium to create distance between the tip and the surface.

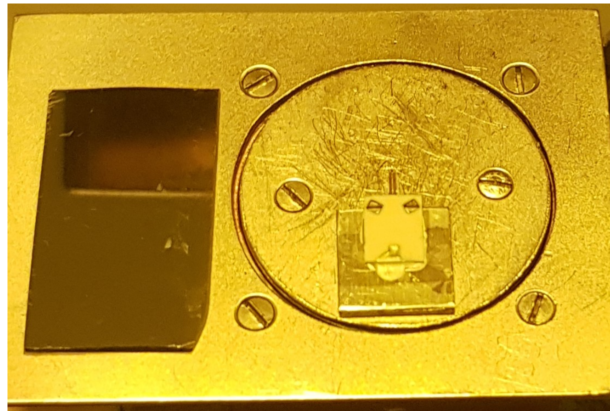

Figure 3.10: *Probe placed on an aluminium plate on top of the etcher sample holder. Based on the same method as Matthijs Rog. The probe is placed on top of an aluminium plate held with silver paint. The aluminium plate is again held by silver paint. The tip is pointing towards the sample holder.*

In figure 3.10 the etching method based on the method of Matthijs Rog [11] is shown. This method uses an aluminium plate mounted on the etcher sample holder to create a bit of distance to the holder surface where the probe is mounted. To image whether the etching is successful an SEM image can be taken off the edge of the cantilever. The cantilever is imaged both before and after etching. One of the sides should always be etched while the other should not be etched.

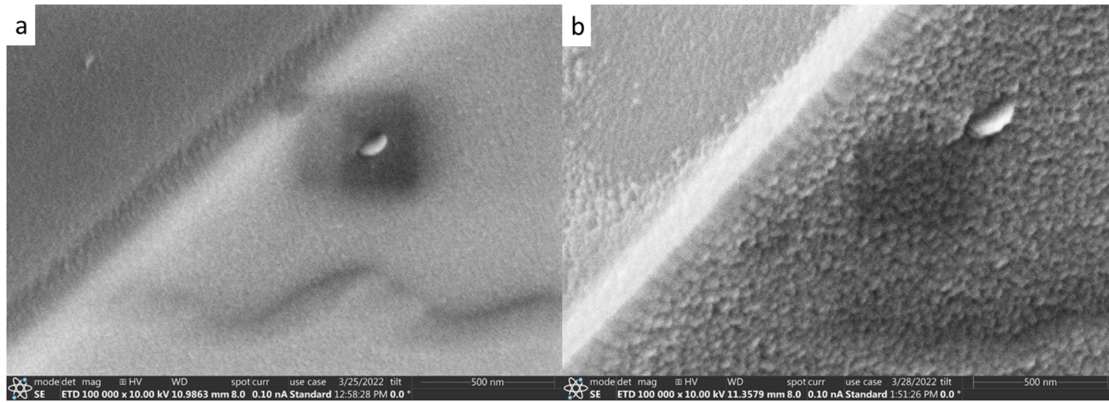

Figure 3.11: *The edge of the cantilever both before (a) and after (b) etching on the aluminium plate as in figure 3.10. The left side of the edge should be etched and the right side should not be etched. After etching the cantilever shows a grainy pattern on both sides.*

In figure 3.11 both a before and after etching SEM image can be seen. The image after etching shows a grainy pattern with a grain size of roughly 50 nm. This is contamination that happens during the etching process since it was not on the cantilever before etching.

The first suspected source of contamination was the silver epoxy both on the base plate holding the tuning fork and on the tuning fork holding the silicon tip. Organic solvents in the epoxy could outgas during the etching process because of the high temperatures. To test this hypothesis it was tried to bake a new cantilever and redo the procedure the same. This turned out to not be the source of contamination because the contamination was still there with similar grain size. It turned out to be caused by unwanted deposition of material from the sample holder during etching.

3.3.3 Deposition During Etching

During the etching process, the beam of argon ions not only hits the cantilever but also the material around it. The argon beam is roughly four centimetres in diameter, which is orders of magnitude larger than the cantilever dimensions. The contamination on the cantilever turns out to be caused by deposition of material that is etched away just around the cantilever.

The sample holder surface of the etcher is made out of stainless steel. The argon ions hit the stainless steel surface, remove material here and the stainless steel is deposited on surrounding materials. Figure 3.12 gives a schematic explanation of this process. The argon ions are coming in vertically. The etcher sample holder is under an angle of 30° with respect to horizontal and so are the aluminium plate and the probe as they are attached with silver paint on this surface. The argon ions hit the stainless steel surface, remove material here (in the figure shown in red) and the material deposits on the cantilever and other surfaces surrounding it.

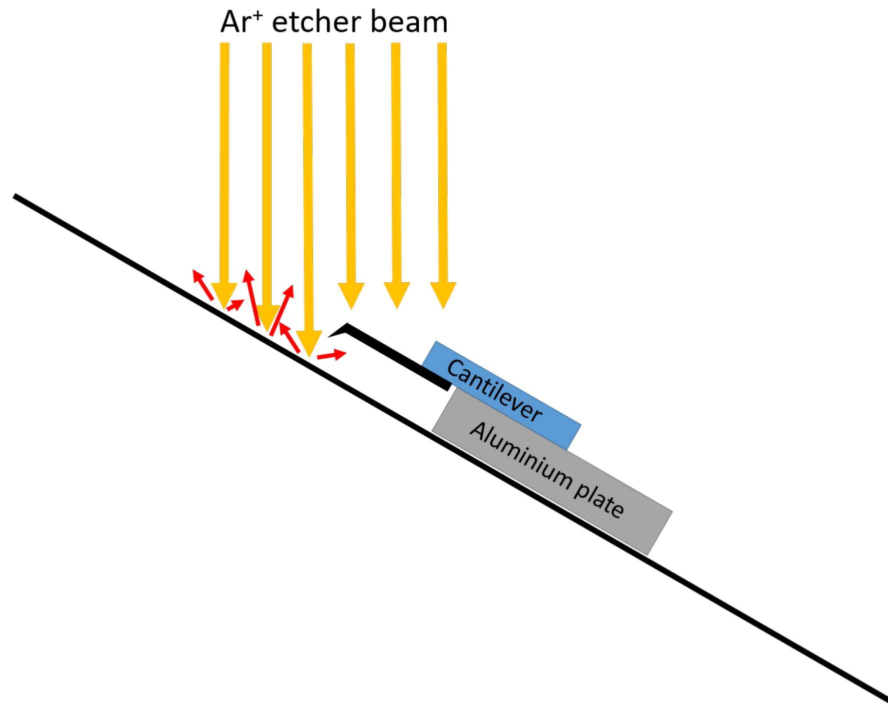

Figure 3.12: *A schematic explanation of the unwanted deposition of stainless steel from the etcher sample holder during the etching process. Argon ions hit the surface (yellow arrows), remove material (shown as red arrows) and this material ends up on the cantilever and other surrounding surfaces.*

A solution to this unwanted deposition could be to increase the distance between the sample holder and the cantilever. The energy of the argon ions determines up to what distance the deposition will appear. If the distance between the sample holder and the cantilever is large enough the problem is solved. This can be done by designing a new sample holder to mount on the existing sample holder.

3.3.4 Etcher Sample Holder

To mitigate the unwanted deposition during etching a new sample holder for the etching process is designed. This holder is meant to replace the aluminium plate and mount it on the existing sample holder of the etcher.

There are three main considerations for the new holder: (a) increasing the distance as discussed before, (b) mounting the cantilever such that the backside of the cantilever is perpendicular to the argon beam and, (c) functioning as a heat sink. The temperature of the probe during etching is unknown but to prevent it from getting too hot the holder will function as a heat sink. This is why the sample holder is made out of copper. This holder design is schematically shown in figure 3.13a.

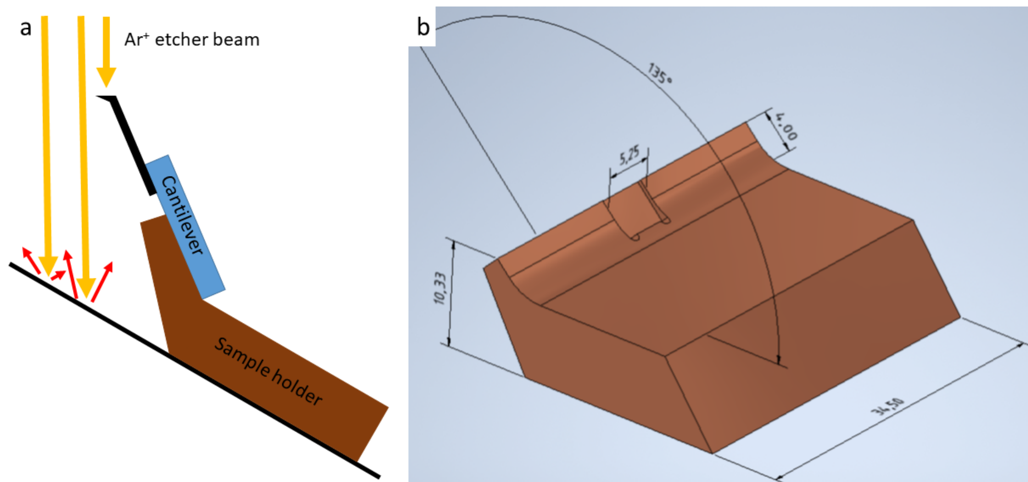

Figure 3.13: *(a) The schematic of the holder for the etching process. The holder increases the distance to the surface to eliminate the deposition during etching. The backside of the cantilever now is perpendicular to the argon beam. The sample holder also functions as a heat sink. (b) The design of the etcher holder drawn in graphical 3D software. The angles make sure the backside of a mounted cantilever is oriented perpendicular to the etcher ion beam. Cantilevers can be mounted using silver paint.*

In figure 3.13b the 3D design of the etcher holder is given. As mentioned the angle under which the probe is mounted results in the backside being perpendicularly aligned to the argon beam. The thickness is chosen such that the maximal volume of copper can be used as a heat sink. The width of the holder is chosen with the same purpose, the maximal width which fits to have maximal heat capacity.

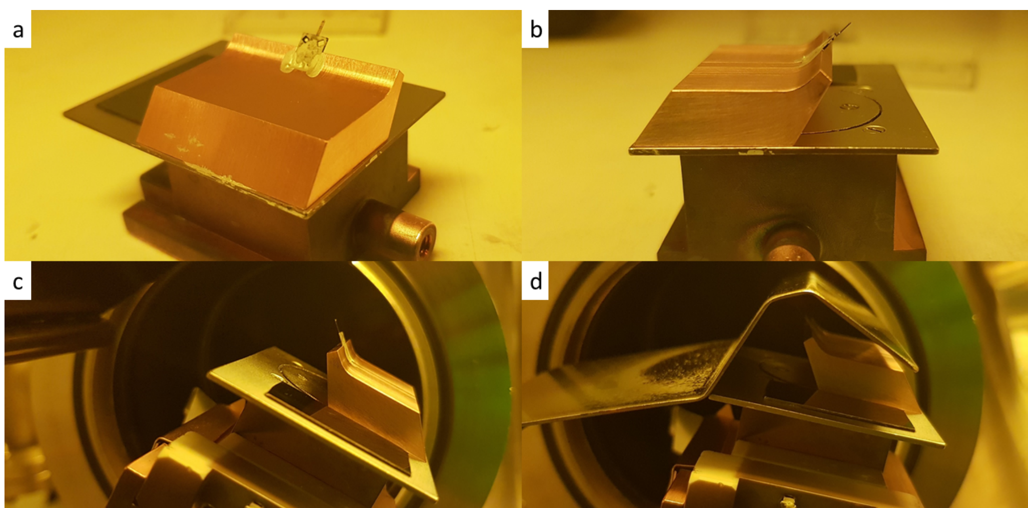

Figure 3.14: *Images of the designed etcher sample holder. First on a table front view (a) and side view (b). Secondly on the etcher stage, ready to slide into the etcher vacuum chamber, without lid (c) and with lid (d). The etcher holder is mounted using silver paint and the probe is also mounted using silver paint.*

The etcher sample holder is mounted on the existing sample holder of the etcher. This is done using silver paint for thermal conductivity. The probes are mounted on the new holder also using silver paint for thermal conductivity. Images of the new sample holder mounted on the original holder are shown in figure 3.14.

After etching the cantilever tip is imaged using the SEM. The results after etching are shown in figure 3.15. These images can be compared to the images in figure 3.11. Both are zoomed in on the same location on the tip, as the rectangle in figure 3.15a indicates.

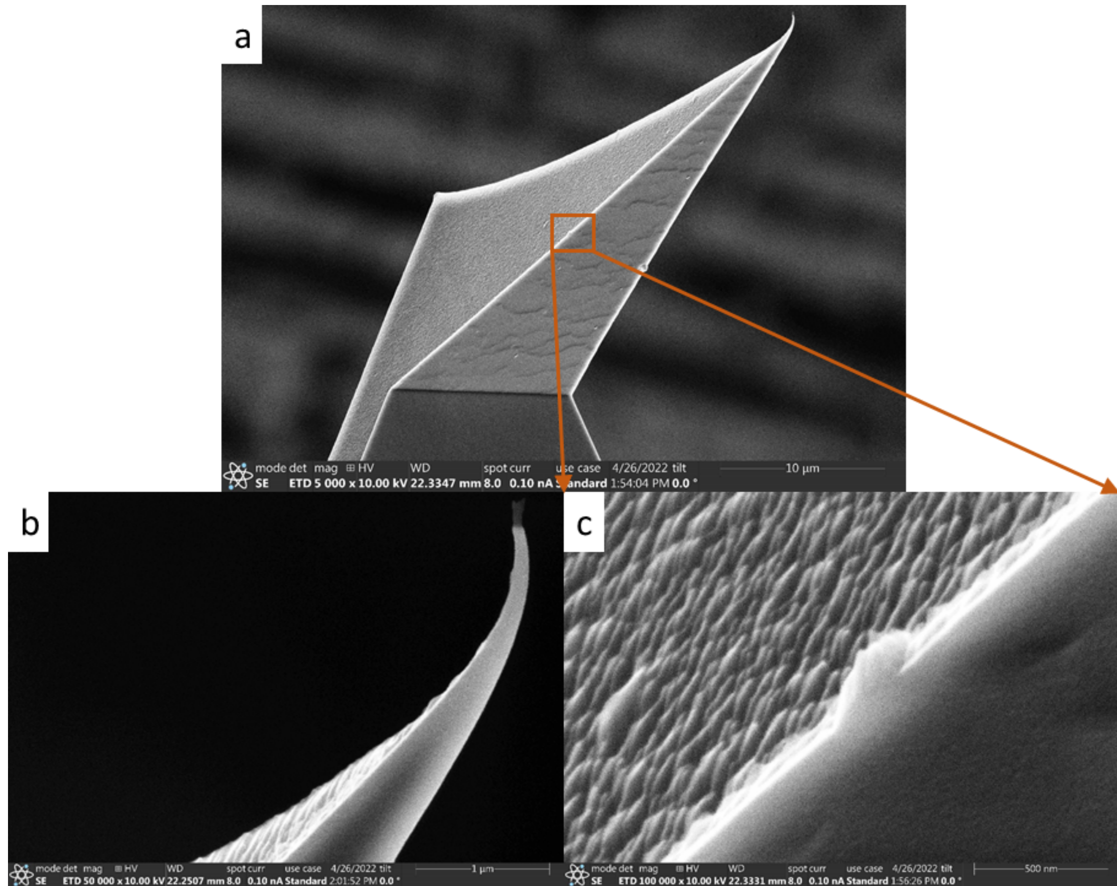

Figure 3.15: *SEM images of the cantilever tip after etching. Before etching the tip looked similar to fig. 3.11a. The overview (a) is given, a zoomed-in view at the tip (b) is given and a zoomed-in view halfway the cantilever is given (c).*

The images in figure 3.15 are the desired results. The inner side of the cantilever is not etched, it is still smooth and at the backside, the conductive material is removed. The backside looks still grainy with a grain size of roughly 50 nm, but this does not matter for creating a SQUID at the inner side. On the end of the tip, there is a thin piece of material left. This is due to over-etching. All material is removed from the backside towards the inner side. In this case, there is still a thin piece of material left

that formerly belonged to the inner side.

The cantilever tip now is etched correctly. However, an inspection by eye of the base plate shows that the problem is now moved to another location. Figure 3.16 shows deposition which is present after etching and was not there before etching. This turns out to be also caused by deposition during the etching process. The horizontal line between the two arrows is also exactly where the edge of the etcher holder is. An electrical resistance measurement also shows that both the two gold contacts and the two SQUID contacts are now shorted. The deposition on the base plate needs to be prevented.

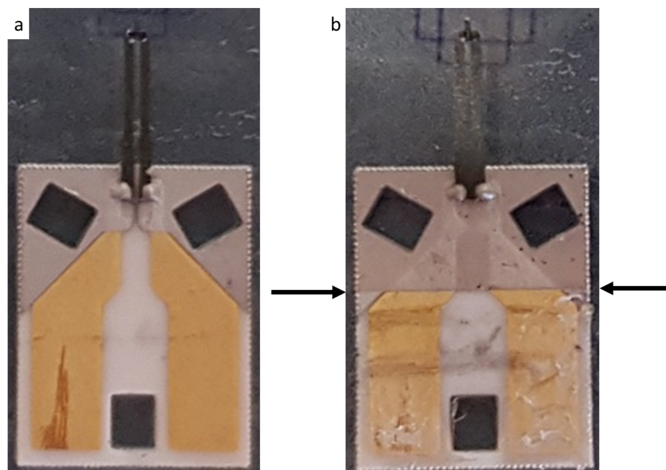

Figure 3.16: *Images of a cantilever before (a) and after (b) etching. The arrows in the right-hand figure indicate up to where the new deposition is. This line of deposition is exactly where the edge of the etcher holder is.*

There is a solution to solve the problem of deposition at the base plate. Namely to have an insulating material surrounding the cantilever, such that the deposition consists of an insulator instead of a conductor.

Cantilever Surrounded by Insulator

As mentioned a solution is to surround the cantilever with insulating material. The deposition will still take place during the etching process, but as long as this happens with an insulating material the electrical circuits are not shorted and it is not a problem. This is done by covering the existing etcher holder with 300 nm of silicon oxide. Besides that, below the cantilever, the stainless steel of the original holder is still visible. To also have an insulating material below the cantilever a piece of silicon oxide is put below the cantilever.

By looking closely by eye to the tuning fork already some thick, grainy deposition can be seen. To circumvent this effect, a new etcher holder is designed that covers the entire base plate and a part of the tuning fork.

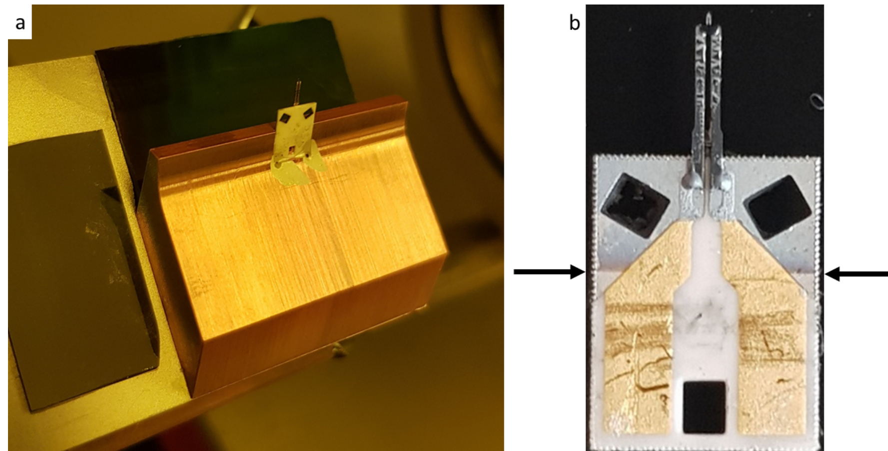

Figure 3.17: *(a) Image of the used etcher holder covered in* 300 nm *of silicon oxide and a silicon oxide plate below the cantilever to prevent an electrical shortage. (b) Image of the result of the etched cantilever. The deposition on the cantilever now changed colour with respect to figure 3.16. The two arrows indicate where the holder ends and where deposition starts.*

New Design of Etcher Holder

A new etcher holder is designed which does not cover only up to somewhere on the base plate but up to the first part of the tuning fork. The holder has to reach up to the same part as the sputter mask does. This ensures that no deposition on the front side can happen up to this part. There will still be deposition at the part that is sticking out. This adds an extra conductive or insulating layer, but this does not matter in practice. In the case of a conductive layer, there will be no additional shortage, only the short at the very end of the cantilever which already existed. This is then milled in two contacts together with the existing layers. In the case of an insulating layer, no additional shortage will appear. There will be an extra layer which can cause the tip to be less sharp. For AFM purposes this is not a favourable development, but in this stadium of developing a SQUID on an AFM tip, it is not relevant.

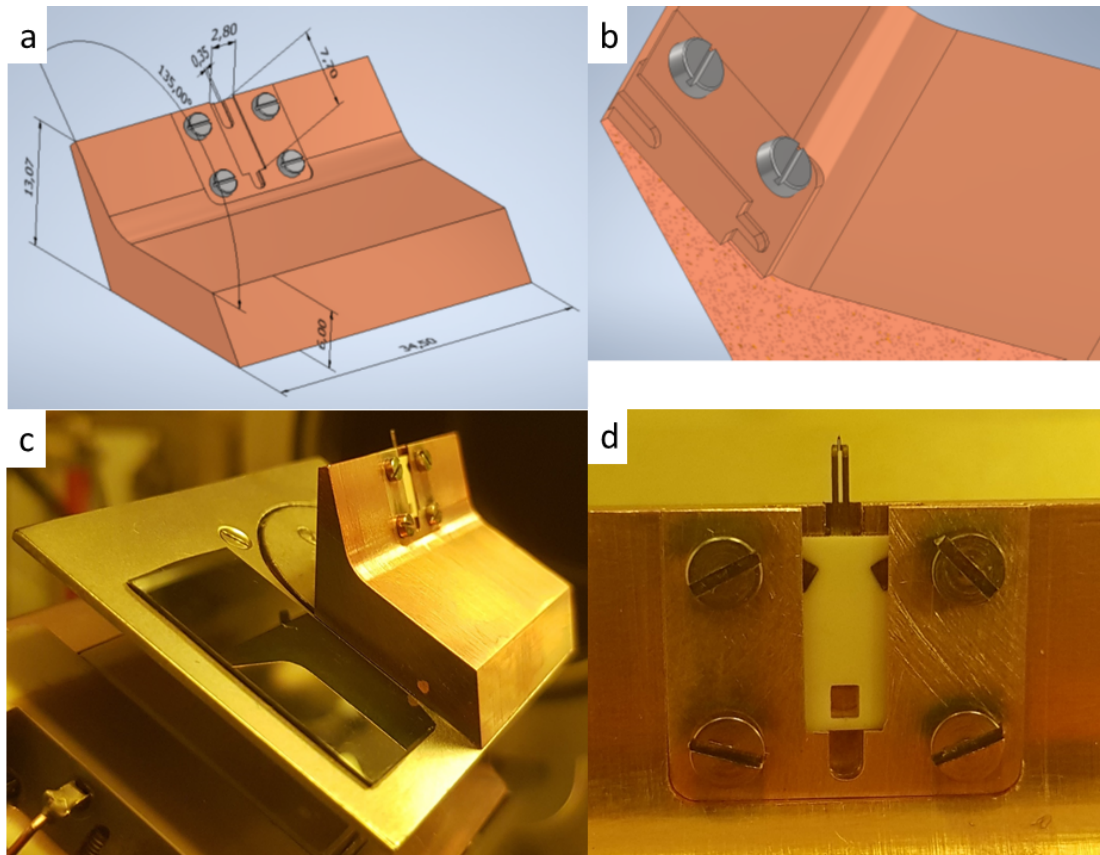

Figure 3.18: *The newly designed etcher sample holder. Two pictures of the designed holder in 3D graphical software, side view (a) and a section (b). Two optical images of the newly designed etcher sample holder. One side view (c) and a zoomed-in view of the part where the probe slides into the holder (d).*

The new design is shown in figure 3.14. This design is based on the old design. As discussed the holder reaches up to the first part of the tuning fork. Furthermore, in the old design, the probes had to be mounted using silver paint. To eliminate the need for silver paint there is a slit that the probe can slide into. This slit can be tightened by four screws if necessary. The holder is during the etching process not used upside down, so in principle, it is not necessary to tighten the probe.

After trying out the new etcher holder it turned out that it is best to also cover this holder in a layer of insulating material. This new holder was therefore covered in 300 nm of silicon oxide.

The result of an etched cantilever using this new etcher holder is given in figure 3.19 and figure 3.20. The shadow of the new etcher sample holder is visible in figure 3.19a as a vertical line. The tip now looks smooth on the inner side and etched at the backside, see figure 3.19b-d.

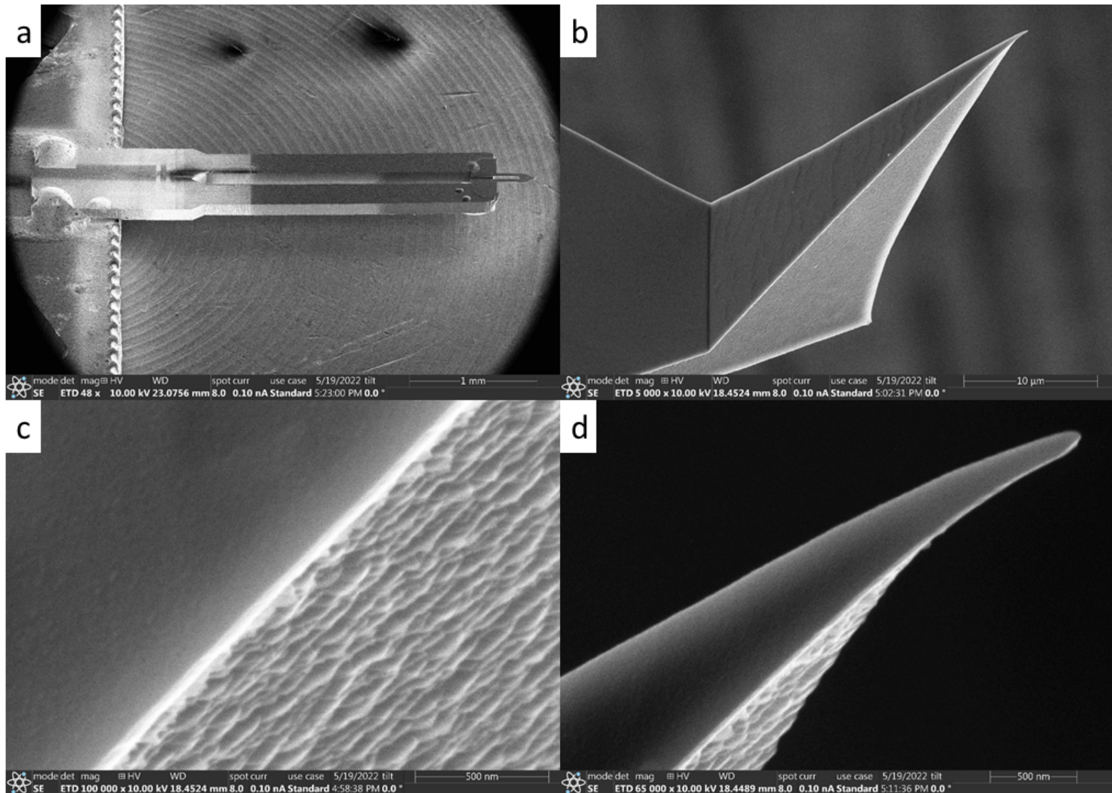

__Figure 3.19:__ Cantilever etched with the new etcher holder. The new holder leaves a shadow visible in (a) on the tuning fork, visible as a vertical line. An overview of the tip in (b). (c) Zoomed in halfway at the tip. The left (inner) side is not etched and the right (back) side is etched as it should be. (d) Zoomed in on the tip. The inner side is smooth and the backside is etched.

Figure 3.20 shows an optical inspection of the etched cantilever. This optical inspection shows that the result with the new etcher holder is now clean. This means that the etching process is now successful.

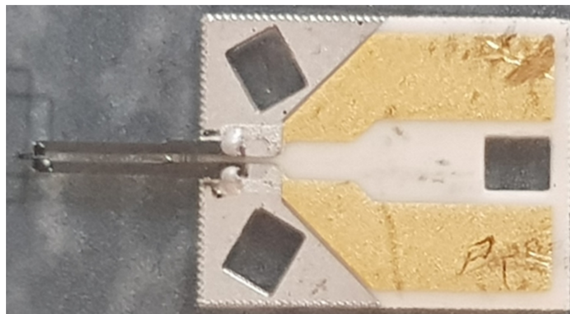

__Figure 3.20:__ An optical inspection of an etched cantilever using the new etcher holder. The cantilever is now clean after etching.

3.3.5 Shorted Electrical Contacts

All steps to make electrical contacts are now thought out and the required sputter mask and the new etcher holder are ready to use. But it turns out there is a problem, the electrical contacts are shorted.

The two AFM electrical contacts should be insulated from each other and they should be insulated from the two sputtered SQUID contacts. The two sputtered SQUID contacts should be insulated from the two AFM contacts and they should be connected via the sputtered electrical path which runs via the tip. By simply measuring the electrical resistance using a multimeter between these four contacts it turns out that this is not the case. All four contacts have a finite resistance between one contact and the other three.

It took a while to figure out this problem and the solution to this problem was not clear. All steps in the sputtering and etching procedure were checked step-by-step to identify the problem.

Short at Silicon Oxide Layer

The first step, sputtering the insulating silicon oxide layer, already created a short. This process is schematically shown in figure 3.21.

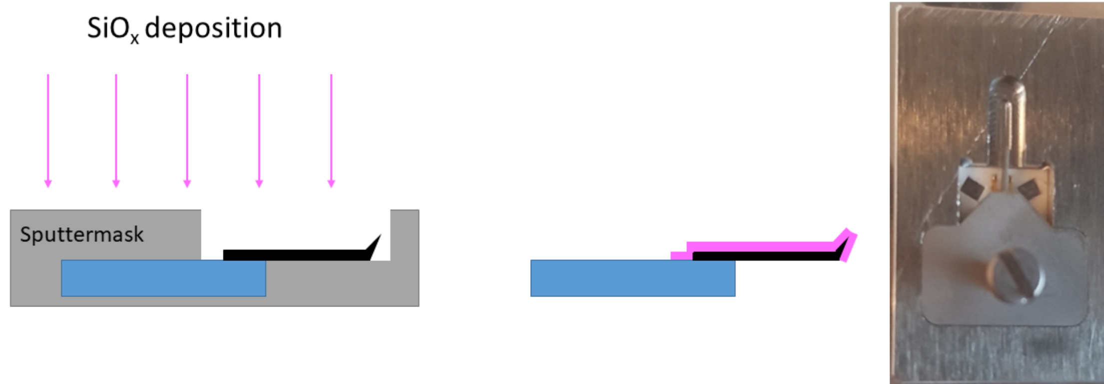

Figure 3.21: *The schematic procedure of sputtering the insulating silicon oxide layer using the sputter mask.*

It was thought that during the sputtering of the silicon oxide layer also some of the conductive metal of the sputter mask was sputtered on the cantilever. This is comparable to the unwanted deposition during etching effect. The short was solved by placing the cantilever on top of a silicon oxide plate instead of in the sputter mask. Now the cantilever is covered everywhere in silicon oxide, not only below the multilayer. See figure 3.22.

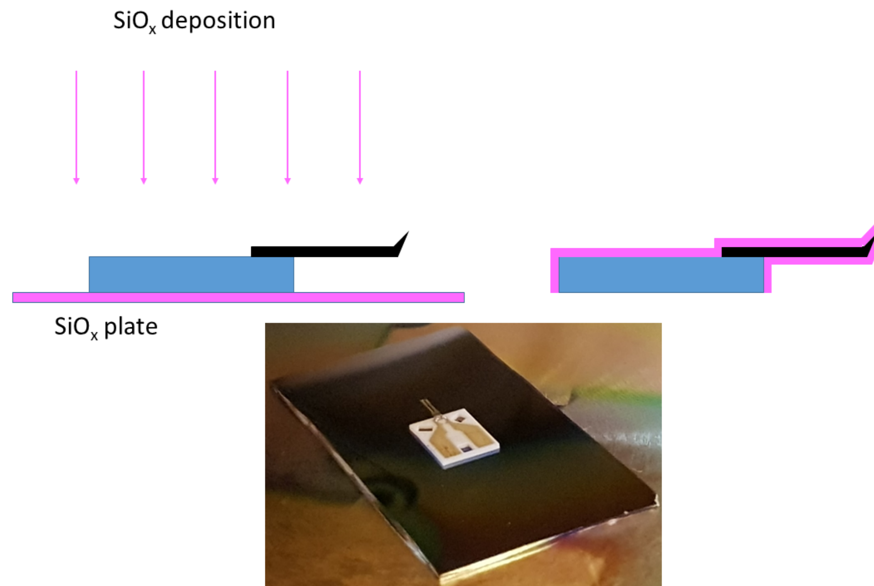

__Figure 3.22:__ The schematic procedure of sputtering the insulating silicon oxide layer using just a piece of silicon oxide.

This has solved the short in the first step, now after sputtering the silicon oxide layer the two gold contacts are electrically isolated.

Short at Multilayer

The next step in the process is the deposition of the multilayer (the MoGe/Pt/MoGe/Pt layers). The gold contacts on the cantilever should be isolated from whatever is sputtered on top in theory, because the silicon oxide layer is separating them. It turns out that this is not the case. Sputtering the multilayer is schematically shown in figure 3.23.

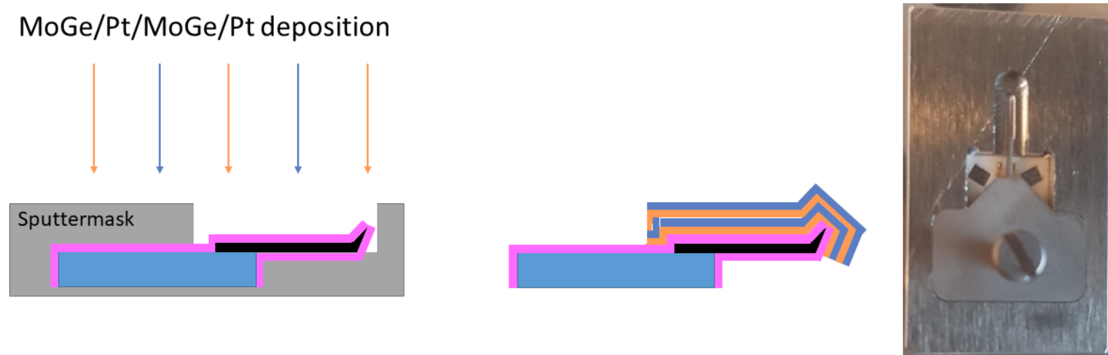

__Figure 3.23:__ The schematic procedure of sputtering the multilayer (MoGe/Pt/MoGe/Pt) on top of the insulating silicon oxide layer using the sputter mask. Please note: the multilayer bends in reality around the tip of the cantilever.

When measuring the electrical resistance after the deposition of the multilayer there are shorts between the sputtered contacts and the AFM contacts which should not be there. Furthermore, the resistance between the two sputtered contacts is also lower than expected.

It was thought that again there is unwanted deposition of the sputter mask during the sputtering process which causes these shorts. To solve this problem a layer (300 nm) of silicon oxide is sputtered on the sputter mask. This did not solve the problem. Two extra layers of both 200 nm were added to the mask, in total adding up to 700 nm of silicon oxide. Still, this step in the process created shorts.

Something else which was noticed are the silver flakes in the silver epoxy moving around somewhere in the process. Two SEM images were taken of the silver epoxy, one before depositing the multilayer (after sputtering the silicon oxide layer) figure 3.24a and one image after deposition of the multilayer figure 3.24b.

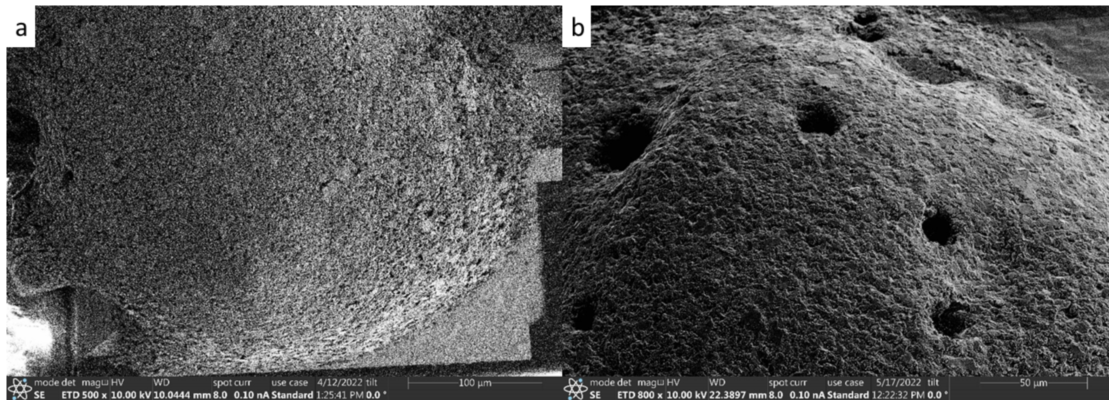

Figure 3.24: *Two SEM images of the silver epoxy. (a) An SEM image before deposition of the multilayer (after sputtering the silicon oxide layer). (b) An SEM image after deposition of the multilayer.*

By the time this short was well known the project ran out of time. Unfortunately within the time of the project, there was no solution found for this problem. This is where the story ends for creating electrical contacts to the tip of the Akiyama-Probes.

As stated in section 3.1 two techniques are known suitable for creating a SQUID on a tip. Now, these techniques are discussed.

3.4 SQUID on Tip

There are two different techniques known to create a SQUID of the desired dimensions on a tip. The first one is to use Focussed Ion Beam (FIB) milling to create the superconducting sides and the weak links in between. The other option is to directly write a SQUID by Electron Beam Induced Deposition (EBID).

3.4.1 FIB SQUIDs

The method using FIB milling is based on the work done by Matthijs Rog. In his thesis, a method is developed for creating a SQUID on an STM tip using FIB milling.

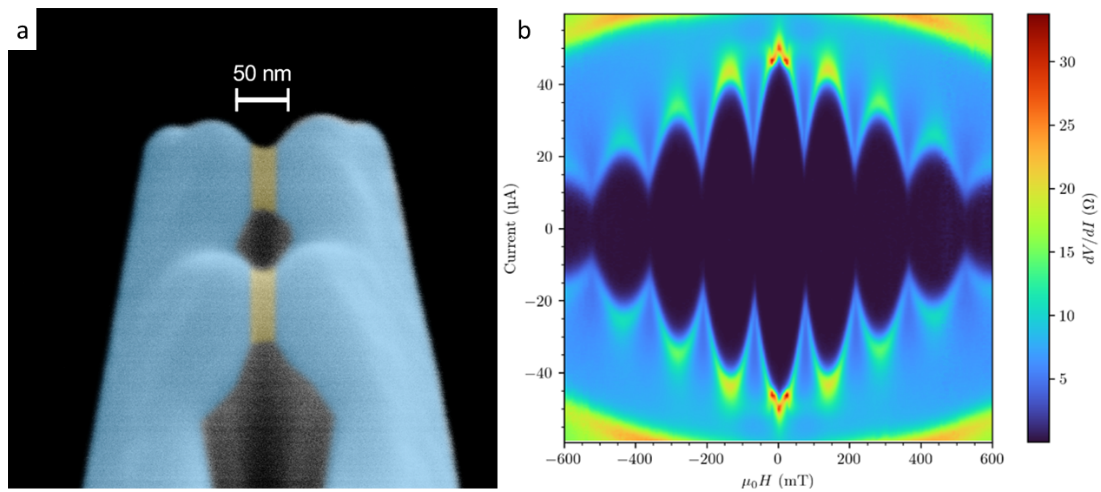

Figure 3.25: *(a) A false-coloured SEM image of the SQUID made by Matthijs Rog. The weak links are coloured yellow and the superconductor is coloured blue. (b) Field sweep measurement of the SQUID on tip as imaged in (a). Adapted from [11].*

Figure 3.25 shows both a false-coloured SEM image of the SQUID on an STM tip made by Matthijs Rog. The weak links are less than 50 nm. The magnetic field sweep clearly shows SQUID oscillations. For further details see the thesis of Matthijs Rog [11].

The same method of making a SQUID on tip can be applied to the Akiyama-Probes as discussed earlier in this chapter. If the preparation of the Akiyama-Probes was successful, i.e. no electrical shorts, the part that needs to be milled is significantly smaller. This would reduce production time significantly.

3.4.2 EBID SQUIDs

Direct writeable SQUIDs using EBID have been developed firstly by Timothy van den Berg [12], shown in figure 3.26a and b. Later on, the design has been changed and made more compact by Tünde de Vries [13], shown in figure 3.26c and d.

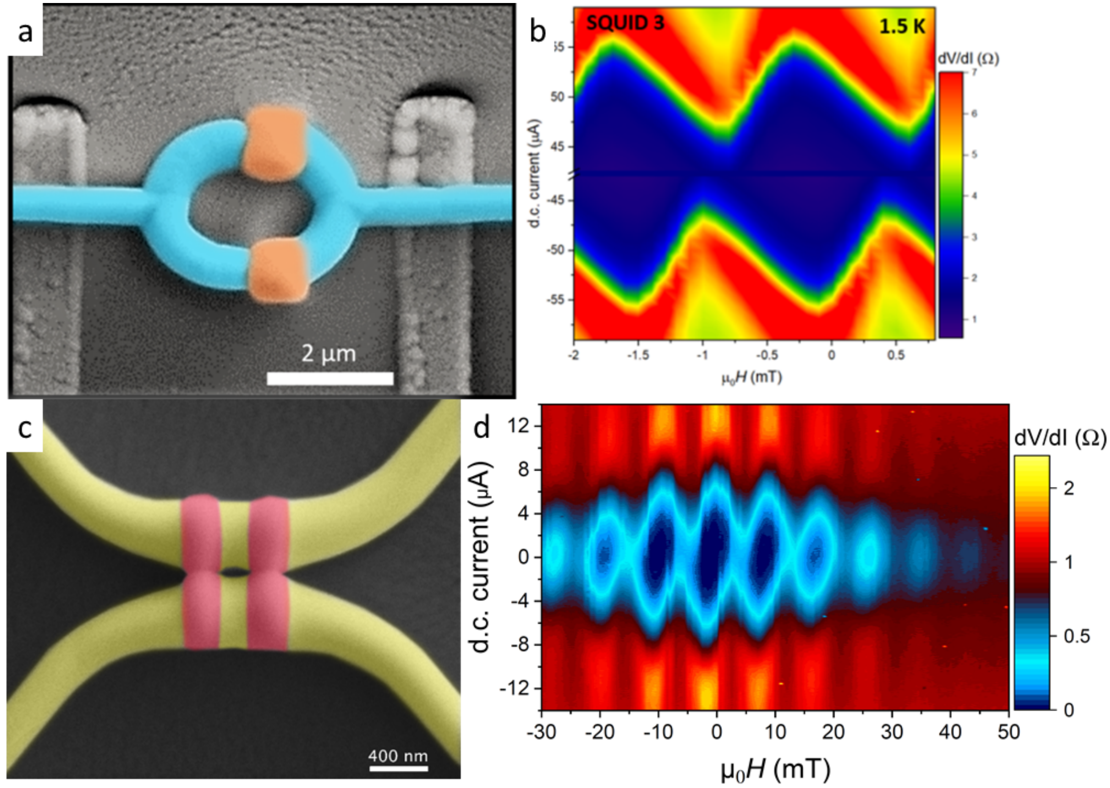

Figure 3.26: *The two EBID SQUIDs of Timothy van den Berg (a) and (b) and Tünde de Vries (c) and (d). (a) A false-coloured SEM image with the superconducting parts in blue and the weak links in orange. (b) The measured magnetic field dependence of the SQUID in (a). (c) A false-coloured SEM image with the superconducting parts in yellow and the weak links in pink. (d) The measured field dependence of the EBID SQUID in (c).*

The design made by Tünde de Vries results in a smaller SQUID which is more applicable on a tip than the larger design made by Timothy van den Berg. The design of Tünde, therefore, is chosen to be firstly optimized and to create the SQUID on the AFM tip.

To be able to create a functional EBID SQUID on the tip it is easiest to first make EBID SQUIDs on planar devices. When making the SQUIDs firstly on planar devices the best parameters for the weak links can be found. The optimized settings then can be applied for a SQUID on a tip.

The first problem encountered was the mismatch of the weak links with respect to the superconducting wires. In figure 3.27a such a device is shown. The mismatch occurred only when printing these devices on top of the gold contacts that are also visible in the SEM image. Printing the devices on a piece of the substrate without the contacts did not result in this mismatch.

This problem was solved by adding a constant shift between the weak links and the superconducting wires. This now results in matching weak links and superconducting wires if the device is printed on top of the gold contacts. If the device is printed on a piece of the substrate without contacts this shift now results in a mismatch. An example of a device with matching weak links is given in figure 3.27b.

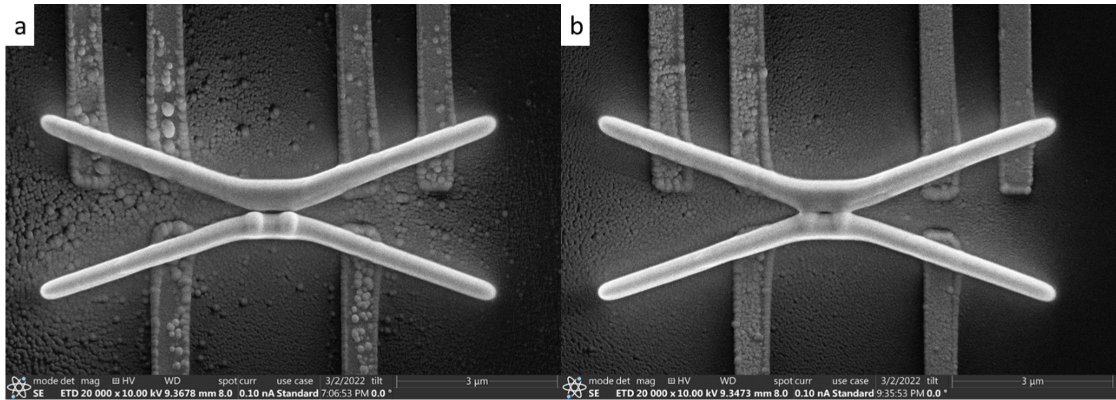

Figure 3.27: *SEM images of two planar EBID devices. First (a) with a mismatch between the weak links and the second (b) with properly matched weak links and superconducting wires.*

By adding this constant shift the weak links continued to appear in the correct location within the same SEM session. In total nine devices were created on top of the gold contacts with the weak links in the correct location. These devices all have different parameters at the weak links for the dwell time and the number of passes, to optimize the SQUID behaviour. In appendix A a table with all printing parameters and images of all devices are given.

These devices were all on the same substrate and they were sent to the University of Tübingen. Both research groups collaborate on this topic and at the time it was more time-efficient to measure the devices in Tübingen. At the time of writing the thesis, the transport results are not in. Therefore they cannot be found in this thesis.

3.4.3 Preliminary Tests on an AFM Tip

In parallel with finding the optimized parameters for the EBID SQUIDs, a preliminary test was done on an AFM tip. This was done to determine whether doing EBID on a tip causes additional problems which are absent on a planar device.

The first challenge was to align the gas nozzle to the tip. At planar devices, this is done by touching the substrate with the gas nozzle and then moving away from the substrate. This is not possible with the AFM tips because these are too fragile for this. After all the alignment was done by eye in the SEM. This turned out not to be a problem, but by doing it by eye it is less reproducible than in the case of planar devices.

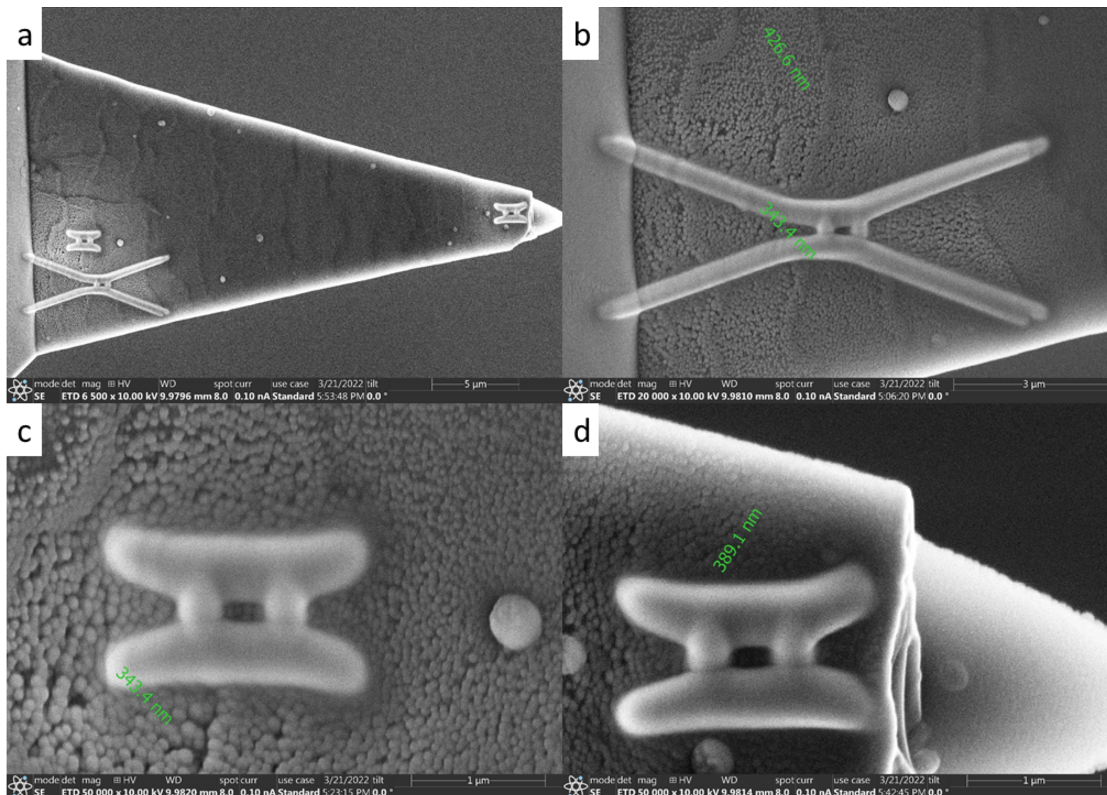

Figure 3.28: *Three tests of EBID devices on a tilted AFM tip. (a) Overview of the three tests on the AFM cantilever. Viewed tilted from the inner side. (b) Test 1, the same pattern as on the planar substrate was used. (c) Test 2, the wires were made shorter. (d) Test 3, the pattern was created close to the edge of a broken tip. In all three cases, the weak links are not perfectly aligned with the wires.*

In total three tests were done on the inner side of a sputtered Akiyama-Probe. These are shown in figure 3.28. The first test was done with the same pattern as used on a planar device. The weak links were shifted to the right with respect to the wires. During imaging, a constant drift of the tip was visible to the left. This is because the tip is now mounted on a 45° angle to have the inner side of the cantilever near horizontal. The tip

is attached using carbon paint. The cantilever slowly drifts because of the gravitational forces.

The length of the wires was decreased for the second test. This was to both decrease the time it takes to create the pattern and to make the structure smaller. By decreasing the printing time, the time between printing the wires and the weak links is also decreased. Since the drifting of the AFM tip is proportional to time the mismatch between the weak links and the wires is now also decreased. Besides the mismatch, the structure also does not have to be that large on the tip. The device in the second test is now roughly 1.2 µm in the vertical direction and 2.0 µm in the horizontal dimension. This is orders of magnitude larger than the end of the tip. In this test, the end of the tip was broken, so it can be placed very close to the end of the tip.

The third and last test was the same pattern as in the second test but now as close to the end of the tip as possible. The pattern ended up exactly where it was expected. Still, there is a little mismatch between the weak links and the wires. This mismatch is solvable by adding a constant shift between the two. Because of the mismatch, the right weak link also looks very thin. The distance between the wires is larger there so the weak link gets spread out a bit and this results in a thin part in the middle.

These preliminary tests have shown that placing EBID devices on a sputtered AFM cantilever is possible. The shift of the weak links with respect to the wires is solvable. The drift is also preventable by making a new holder for in the SEM. In that case, it can rest on a part of the holder instead of only being held by carbon paint.

Chapter 4

Conclusion & Outlook

SQUID on tip microscopy is a technique that provides a way to investigate many interesting sorts of physics. The SQUID is sensitive to both magnetic fields and temperature. This enables the opportunity to very accurately and very locally measure magnetic fields and temperature on a nanometre spatial scale. Current SQUID on tip measurements suffer from a lack of proper height control which results in limited sensitivity and spatial resolution.

In this thesis, a solution to this problem is suggested by applying the SQUID on tip principle on an Atomic Force Microscopy (AFM) cantilever. This combination provides effective height control for the SQUID on tip and it provides the opportunity to collect topographic information besides the magnetic and thermal information from the SQUID.

A method is designed to realize this solution, the combination of a SQUID on an AFM tip. The method is based on starting with a commercially available cantilever (Akiyama-Probe), sputtering an insulating layer and four conductive layers on top (4 nm MoGe, 25 nm Pt, 55 nm MoGe, and4 nm Pt), etching away the part which would short the SQUID (backside) and finally creating a SQUID by either Focussed Ion Beam (FIB) milling or Electron Beam Induced Deposition (EBID).

Various challenges were encountered while designing this method. Several of these challenges were overcome in this thesis, but there is one challenge left at the end. Electrical shorts between the four electrical contacts (two gold AFM contacts and two sputtered SQUID contacts) are the reason that there is no functional AFM SQUID on the tip at the end of the project.

Cooling the cantilever down could (partially) solve the problem of the electrical shorts. At low temperatures, the resistance of the shorts increases while the superconducting circuit will decrease in resistance. This could make the electrical circuit operational if the desired electrical path is energetically more favourable than the path via the short.

The silver epoxy attaching the base plate and the tuning fork is hypothesized as the reason behind the electrical shorts. The flakes of silver epoxy seem to move during some step in the process, however, no clear explanation for this has been found (yet).

In the future, the electrical shorts need to be solved. This could be done for example by covering the mentioned silver epoxy with a layer of Torr Seal. This would also act as an insulating layer and hopefully prevent the shorts.

Supposing the electrical shorts are mitigated, a new interesting microscope technique opens up. This technique can be used to measure the topography of the surface, the magnetic properties of the sample, and electrical currents and dissipation in the material, all parallel to each other.

References

[1] P. Reith, X. Renshaw Wang, and H. Hilgenkamp, *Analysing magnetism using scanning SQUID microscopy*, Review of Scientific Instruments **88**, 1 (2017).

[2] A. Finkler, *Scanning NanoSQUID Microscope for Study of Vortex Matter in Type-II Superconductors*, PhD thesis, 2011.

[3] F. S. Wells, A. V. Pan, X. R. Wang, S. A. Fedoseev, and H. Hilgenkamp, *Analysis of low-field isotropic vortex glass containing vortex groups in YBa2Cu3O7-x thin films visualized by scanning SQUID microscopy*, Scientific Reports **5**, 1 (2015).

[4] J. A. Bert, B. Kalisky, C. Bell, M. Kim, Y. Hikita, H. Y. Hwang, and K. A. Moler, *Direct imaging of the coexistence of ferromagnetism and superconductivity at the LaAlO3/SrTiO3 interface*, Nature Physics **7**, 767 (2011).

[5] D. Halbertal, J. Cuppens, M. B. Shalom, L. Embon, N. Shadmi, Y. Anahory, H. R. Naren, J. Sarkar, A. Uri, Y. Ronen, Y. Myasoedov, L. S. Levitov, E. Joselevich, A. K. Geim, and E. Zeldov, *Nanoscale thermal imaging of dissipation in quantum systems*, Nature **539**, 407 (2016).

[6] E. Marchiori, L. Ceccarelli, N. Rossi, G. Romagnoli, J. Herrmann, J. C. Besse, S. Krinner, A. Wallraff, and M. Poggio, *Magnetic imaging of superconducting qubit devices with scanning SQUID-on-tip*, page 1 (2022).

[7] J. R. Kirtley, *Fundamental studies of superconductors using scanning magnetic imaging*, Reports on Progress in Physics **73** (2010).

[8] J. Clarke and A. I. Braginski, *The SQUID Handbook*, volume 1, 2005.

[9] NanoSensors, *Akiyama-Probe Specifications.*

[10] T. Akiyama, U. Staufer, N. F. De Rooij, P. Frederix, and A. Engel, *Symmetrically arranged quartz tuning fork with soft cantilever for intermittent contact mode atomic force microscopy*, Review of Scientific Instruments **74**, 112 (2003).

[11] M. Rog, *SQUID-on-tip Magnetic Microscopy using Tunneling-Based Height Control (MSc thesis)*, 2022.

[12] T. V. D. Berg, *Direct-write Printed Superconducting QUantum Interference Devices using Focused Electron Beam Induced Deposition (MSc thesis)*, 2021.

[13] T. L. D. Vries, *Printing electrically tunable SQUIDs (BSc thesis)*, 2021.

Appendix A

EBID Planar Devices Parameters

As mentioned in subsection 3.4.2 the parameters and images of all planar EBID devices are given below. Only the ones where the weak links matched the wires are listed.

Type of Structure	Detector Mode	Substrate	HV (kV)	Beam (nA)	Dwell (ms)	Passes	Time (m:s)	Pitch (nm)	Scan Direction	Dimensions	Overlap	Pstart (mBar)	Pend (mBar)
SQUID wires	standard	4G	10	20	25	2	15:32	0.93	Perpendicular	see text	98%	1.04E-6	1.00E-5
SQUID weak links	standard	4G	10	20	4	40	00:31	20	Left to right	$0.12 \times 0.32\,\mu m$	60%	1.10E-6	9.91E-6
SQUID wires	standard	4H	10	20	25	2	15:32	0.93	Perpendicular	see text	98%	1.02E-6	9.91E-6
SQUID weak links	standard	4H	10	20	4	45	00:35	20	Left to right	$0.12 \times 0.32\,\mu m$	60%	1.11E-6	9.82E-6
SQUID wires	standard	4I	10	20	25	2	15:32	0.93	Perpendicular	see text	98%	1.06E-6	9.67E-6
SQUID weak links	standard	4I	10	20	4	50	00:38	20	Left to right	$0.12 \times 0.32\,\mu m$	60%	1.08E-6	9.82E-6
SQUID wires	standard	4J	10	20	25	2	15:32	0.93	Perpendicular	see text	98%	1.05E-6	9.96E-6
SQUID weak links	standard	4J	10	20	7	26	00:35	20	Left to right	$0.12 \times 0.32\,\mu m$	60%	1.08E-6	9.77E-6
SQUID wires	standard	4L	10	20	25	2	15:32	0.93	Perpendicular	see text	98%	1.04E-6	9.76E-6
SQUID weak links	standard	4L	10	20	7	23	00:31	20	Left to right	$0.12 \times 0.32\,\mu m$	60%	1.07E-6	9.70E-6
SQUID wires	standard	4M	10	20	25	2	15:32	0.93	Perpendicular	see text	98%	1.03E-6	9.82E-6
SQUID weak links	standard	4M	10	20	7	29	00:39	20	Left to right	$0.12 \times 0.32\,\mu m$	60%	1.05E-6	9.87E-6
SQUID wires	standard	4N	10	20	25	2	15:32	0.93	Perpendicular	see text	98%	1.02E-6	9.69E-6
SQUID weak links	standard	4N	10	20	5	36	00:35	20	Left to right	$0.12 \times 0.32\,\mu m$	60%	1.05E-6	9.70E-6
SQUID wires	standard	4O	10	20	25	2	15:32	0.93	Perpendicular	see text	98%	1.01E-6	9.69E-6
SQUID weak links	standard	4O	10	20	5.5	33	00:35	20	Left to right	$0.12 \times 0.32\,\mu m$	60%	1.08E-6	9.67E-6
SQUID wires	standard	4P	10	20	25	2	15:32	0.93	Perpendicular	see text	98%	1.01E-6	9.74E-6
SQUID weak links	standard	4P	10	20	6	30	00:35	20	Left to right	$0.12 \times 0.32\,\mu m$	60%	1.06E-6	9.64E-6

Table A.1: *This table provides the parameters used when creating the nine planar EBID devices. The dimensions of the SQUID wires are determined by the Python code made by Tünde de Vries. The used variables in the Python code are: gap: 2300, lp: 4000, ld: 12000, alpha: 19, curve: 1000 and var: n.*

The SQUID wires were made by creating a Streaming File using the Python code of Tünde de Vries. The Python code and explanation are given in her thesis [13]. The used variables in the Python code resulting in the dimensions here are gap: 2300, lp: 4000, ld: 12000, alpha: 19, curve: 1000, and var: n.

In figures A.1 and A.2 SEM images of all planar EBID devices can be found where the weak links match the wires.

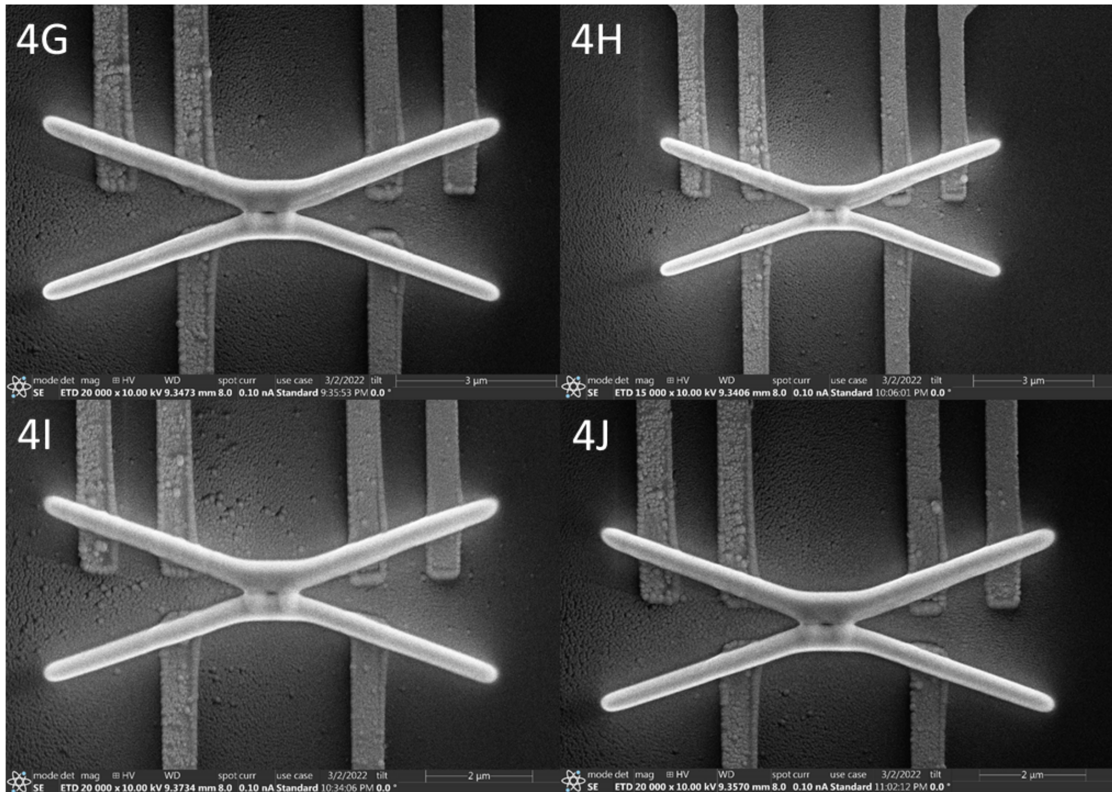

Figure A.1: *SEM images of EBID devices 4G up to 4J.*

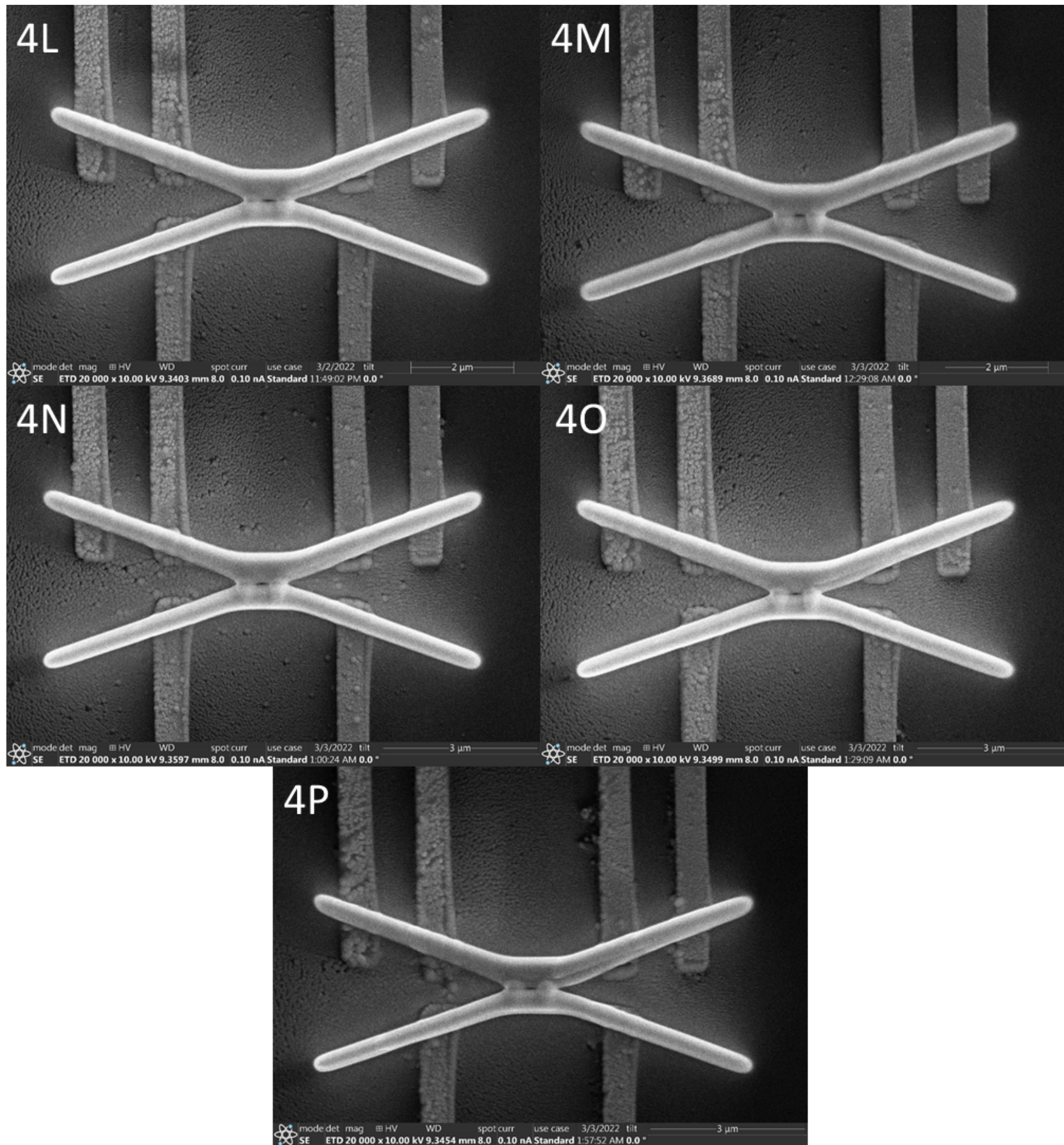

Figure A.2: *SEM images of EBID devices 4L up to 4P.*

Acknowledgments

It would be unfair to take all credits for this master's project and the content of this thesis on my own. Without the help of various people in the institute, all of this would not have been possible. The warm welcome in the research group of Jan Aarts was the start of the story you just read. Without the group, this project would of course not have been possible.

Kaveh Lahabi as a daily supervisor has told me a lot about physics, superconductors, SQUIDs, junctions, and so on. When I was stuck at some point he always knew a way to get me going again. With his new job I wish him all the luck in the world with his new research and above all, with continuing to educate students as he does.

Together with Jimi de Haan, I looked at a lot of the practical problems. It was very useful to have conversations about the physics and the equipment together. He was always in for a quick talk to solve problems quickly.

Roughly the first half of my project I shared an office with Matthijs Rog. He started before me and thanks to him I could start quickly and get things going. He designed the recipes for the SQUID layers which I could directly use, not to mention all other general knowledge I could just use and learn from him.

The research group as a whole has supported my research by answering my questions, helping me with the equipment, and with interesting and joyful conversations during breaks. Therefore I want to thank Jan Aarts, Remko Fermin, Junxiang Yao, Kumar Prateek end Tycho Blom.

Near the end of my project, it was a pleasure that already someone was continuing the research and trying to find the electrical shorts. I helped Zhiyuan Cheng with getting started with his master's project. I hope he learned from me just as I learned from Matthijs.

Last but not least I want to thank all the technical people who I bothered with my questions and my wishes. Douwe Scholma together with Marcel Hesselberth maintained the necessary equipment and were always willing to explain to me something. Hugo van Bohemen from the Fine Mechanical Department designed and made the sputter mask and both etcher holders for me. Without the technicians, all physics research would not be possible.

Scripsi.